AD-A116 105 NAVAL RESEARCH LAB WASHINGTON DC F/G 20/1
FREQUENCY DISPERSION OF SOUND IN UNDERSEA PROPAGATION.(U)
JUN 82 A A GERLACH, K D FLOWERS, R B JOHNSON
UNCLASSIFIED NRL-8600 NL

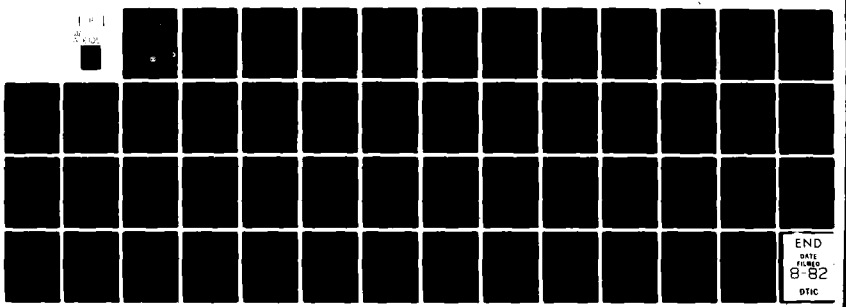

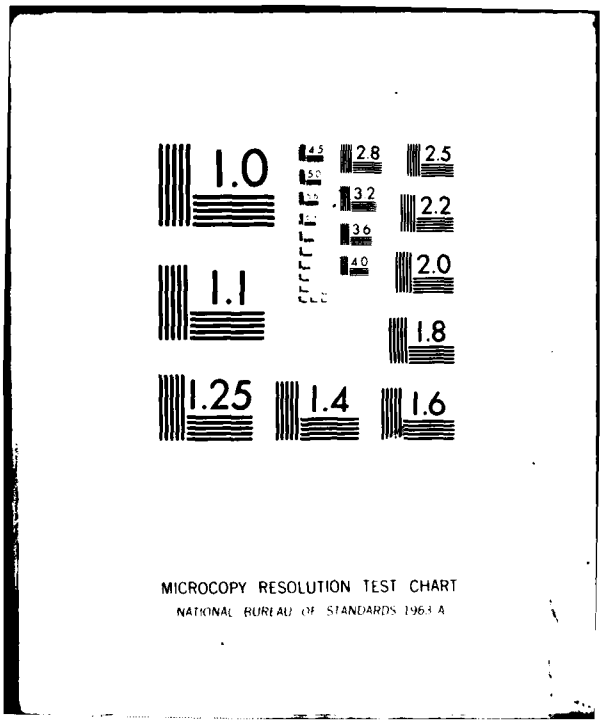
1.0
1.1
1.25
1.4
1.6
1.8
2.0
2.2
2.5
2.8
3.2
3.6
4.0
MICROCOPY RESOLUTION TEST CHART
NATIONAL BUREAU OF STANDARDS 1963 A

Frequency Dispersion of Sound in Undersea Propagation

A. A. GERLACH, K. D. FLOWERS, R. B. JOHNSON, JR., W. L. ANDERSON, AND E. L. KUNZ

Systems Engineering and Advanced Concepts Branch
Acoustics Division

June 17, 1982

NAVAL RESEARCH LABORATORY
Washington, D.C.

SECURITY CLASSIFICATION OF THIS PAGE (When Data Entered)

REPORT DOCUMENTATION PAGE

READ INSTRUCTIONS BEFORE COMPLETING FORM

1. REPORT NUMBER NRL Report 8600	2. GOVT ACCESSION NO. AD-A116705
3. RECIPIENT'S CATALOG NUMBER	
4. TITLE (and Subtitle) FREQUENCY DISPERSION OF SOUND IN UNDERSEA PROPAGATION	5. TYPE OF REPORT & PERIOD COVERED Interim report on a continuing NRL problem
	6. PERFORMING ORG. REPORT NUMBER
7. AUTHOR(s) A. A. Gerlach, K. D. Flowers, R. B. Johnson, Jr., W. L. Anderson, and E. L. Kunz	8. CONTRACT OR GRANT NUMBER(s)
9. PERFORMING ORGANIZATION NAME AND ADDRESS Naval Research Laboratory Washington, DC 20375	10. PROGRAM ELEMENT, PROJECT, TASK AREA & WORK UNIT NUMBERS P.E. 62759N; XF59-552-091; NRL problem 51-1397-0-2
11. CONTROLLING OFFICE NAME AND ADDRESS Naval Electronic Systems Command Washington, DC 20360	12. REPORT DATE June 17, 1982
	13. NUMBER OF PAGES 52
14. MONITORING AGENCY NAME & ADDRESS(if different from Controlling Office)	15. SECURITY CLASS. (of this report) UNCLASSIFIED
	15a. DECLASSIFICATION/DOWNGRADING SCHEDULE

16. DISTRIBUTION STATEMENT (of this Report)

Approved for public release; distribution unlimited.

17. DISTRIBUTION STATEMENT (of the abstract entered in Block 20, if different from Report)

18. SUPPLEMENTARY NOTES

19. KEY WORDS (Continue on reverse side if necessary and identify by block number)

Acoustic propagation
Underwater acoustics
Frequency dispersion

20. ABSTRACT (Continue on reverse side if necessary and identify by block number)

Acoustic dispersion in a deep ocean channel is characterized by the dependence of sound propagation speed on signal frequency along the axial propagation path. A model normal-mode solution of the wave equation is employed to compute the acoustic field for sinusoidal signals as a function of both axial range and frequency. A virtual propagation time is defined, which reflects the range-dependent phase of the acoustic field. When signals of different frequency are transmitted, the remotely observed frequency ratio (for a given range-rate) will fluctuate about the true frequency ratio of the transmitted signals. The magnitude of the fluctuation is directly proportional to the true frequency ratio.

Continued

DD FORM 1 JAN 73 1473 EDITION OF 1 NOV 65 IS OBSOLETE
S/N 0102-014-6601

SECURITY CLASSIFICATION OF THIS PAGE (When Data Entered)

20. ABSTRACT (Continued)

A measure of the spectral dispersion is defined as the difference between the observed and true frequency ratios. The dependence of this measure on range and signal frequencies (for a given frequency ratio) is determined to be relatively insignificant. It is concluded that spectral acoustic dispersion in a deep ocean channel is microscopic, but it can be significant for applications involving the phase correlation of broadband (or spectrally separated) signals over long time intervals.

CONTENTS

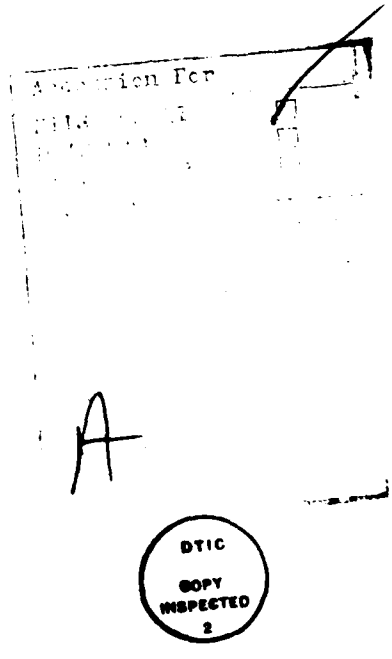

FREQUENCY DISPERSION OF SOUND IN UNDERSEA PROPAGATION

INTRODUCTION

Although the effect of acoustic dispersion in a deep ocean channel is relatively insignificant for narrowband signals, it can become a factor for signals widely separated in frequency. Due to the complexity of the ocean channel, varied approaches have been taken in the study of dispersion in acoustic propagation [1-7]. For applications involving coherence processing of broadband (or widely separated narrowband) signals, the results of Ref. 1 appear most useful. Consequently, a more elaborate study was made of the dispersive effect of widely separated signal sinusoids propagating in a deep ocean channel. A virtual propagation time is defined, which reflects the range-dependent phase of the acoustic field. The virtual propagation time (along with the corresponding axial sound speed) fluctuates both with range and signal frequency. Use is made of the virtual propagation time to calculate the deviation in the observed frequency ratio of two signals relative to the actual ratio transmitted. Although the physical model of the ocean channel is somewhat idealized (for computational simplicity), the statistical results are believed to be representative of those which will be realized in a real ocean environment.

OCEAN-CHANNEL MODEL

The geometry of the ocean channel under consideration is depicted in Fig. 1. The source depth is 150 m, and the receiver depth is 3500 m. The range R is the horizontal distance between the source and receiver in meters. The vertical sound-speed profile is typical of that for the NE Pacific ocean in the late summer, and it is assumed constant over the range under consideration. The ocean bottom (at a depth of 6000 m) is considered perfectly absorbing, and the surface is assumed to be a perfect pressure-release boundary.

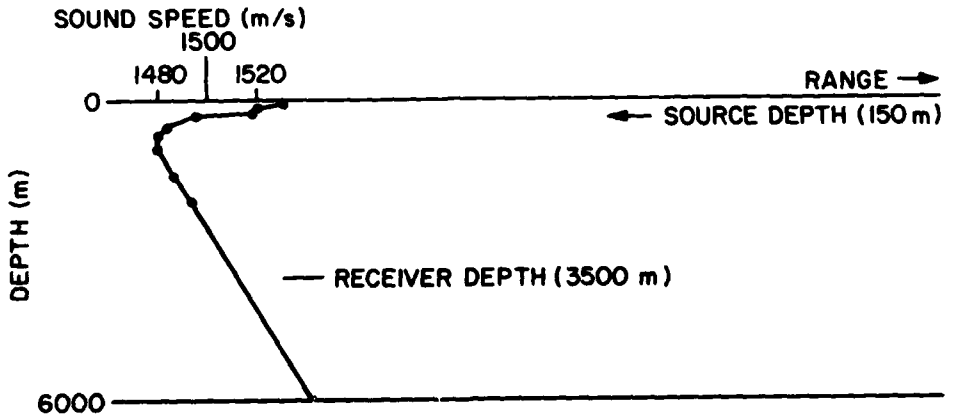

Fig. 1 — Geometry and depth-dependent sound-speed profile used as an ocean-channel model

Manuscript submitted March 15, 1982.

The acoustic field as a function of range R and water depth D (ωt suppressed) is calculated as

$$\psi(R) = A(R) \exp [-i\phi(R)], \tag{1}$$

where

$$A(R) = \sqrt{2\pi/RD^2} \left| \sum_m P_m \exp (ik_m R) \right| \tag{1a}$$

and

$$\phi(R) = \arctan \left[\frac{\sum_m P_m \sin (k_m R)}{\sum_m P_m \cos (k_m R)} \right]. \tag{1b}$$

The mode amplitudes P_m and wavenumbers k_m ($m = 1, 2, \ldots$) are computed using the NRL normal-mode model [8].

The above channel model is the same as that employed in Ref. 1 and, although oversimplified, should give results which are reasonably representative of what can be expected in a real ocean environment.

VIRTUAL PROPAGATION TIME

In an ideal medium, the acoustic field may be expressed as $A(R) \exp [i\omega(t - t_R)]$, where t_R is the propagation time between the source and the receiver. The ocean channel, however, is more complicated and does not lend itself to a strict interpretation of propagation time. This is a consequence of multipath signal arrivals, which give rise to a composite acoustic field. On the other hand, the relative phase of a single frequency may be tracked along the range axis and used to determine the virtual phase-propagation speed along this axis. This can be employed to compute the virtual (or effective) propagation time along the axis if $\omega t_R = 2\pi f t_R$ is related to the phase function $\phi(R)$.

Consider now the use of Eq. (1b) to compute the relative phase of the acoustic field for a sequence of range values $R_n = R_0 + Kn$ ($n = 0, 1, 2, \ldots, N$), where K is sufficiently small to preclude phase ambiguity. To track the phase, define

$$\Delta\phi_n = \begin{cases} \phi(R_n) - \phi(R_{n-1}) & \text{for } -\pi < \phi(R_n) - \phi(R_{n-1}) \leqslant \pi, \\ \phi(R_n) - \phi(R_{n-1}) + 2\pi & \text{for } \phi(R_n) - \phi(R_{n-1}) \leqslant -\pi, \\ \phi(R_n) - \phi(R_{n-1}) - 2\pi & \text{for } \pi < \phi(R_n) - \phi(R_{n-1}). \end{cases} \tag{2}$$

The virtual propagation time between range R_0 and range R_n will be defined as

$$T(R_n; f) = \frac{1}{2\pi f} \sum_{j=1}^{n} \Delta\phi_j, \tag{3}$$

and the average axial phase-propagation speed over the range increment R_j to R_n is

$$\bar{c}_{jn}(f) = \frac{(n-j)K}{T(R_n; f) - T(R_j; f)}. \tag{4}$$

From the above definitions, it is evident that the virtual propagation time is not necessarily a monotonic function of R, but it can either increase or decrease with n, as well as vary with the signal frequency f. This is intuitively acceptable, since the received signal at any range may be viewed as the superposition of signals arriving over several eigenray paths with differing propagation times [9]. However, the general trend of the virtual propagation time will be to increase with range at a rate inversely

proportional to the average axial propagation speed. Consequently, to study the fluctuations of the virtual propagation time over the range R_0 to R_N, the function $\Delta T(R_n;f)$ is defined as

$$\Delta T(R_n;f) = T(R_n;f) - R_n / \bar{c}_{0N}(f). \quad (5)$$

FLUCTUATIONS IN PROPAGATION TIME

For the model ocean channel described earlier, the fluctuations in the virtual propagation time have been computed from Eq. (5) over the range of 50 to 500 nmi for signal frequencies of 10,15,20,30,40, and 80 Hz. The results are illustrated in Figs. 2 through 10. The axial propagation speeds for each 50-nmi increment, as well as over the entire 450-nmi range, are listed in Table 1.

Table 1 — Average Axial Phase-Propagation Speed Computed over 50-nmi Range Increments for Sinusoidal Signals at Six Specified Frequencies

Range	Phase—Propagation Speed (m/s)					
(nmi)	10 Hz	15 Hz	20 Hz	30 Hz	40 Hz	80 Hz
50-100	1522	1522	1524	1521	1520	1521
100-150	1521	1525	1524	1521	1520	1521
150-200	1519	1525	1523	1523	1521	1522
200-250	1519	1525	1525	1523	1520	1523
250-300	1520	1524	1521	1523	1521	1521
300-350	1522	1522	1525	1523	1522	1523
350-400	1519	1526	1525	1523	1521	1522
400-450	1524	1525	1523	1520	1520	1522
450-500	1522	1524	1526	1521	1521	1522
50-500	1521	1524	1524	1522	1521	1522

Each of the nine figures is for a given 50-nmi range increment, and the results of the six signal frequencies are displayed on each figure. Above each graph of $\Delta T(R_n;f)$, the normalized (cylindrical spreading loss suppressed) acoustic-field amplitude $A(R)$ is displayed to show the relationship between the amplitude and the propagation-time fluctuations. (Signal amplitude is plotted on a linear, rather than a dB scale.) It will be noted that the more rapid propagation-time variations occur at ranges at which the signal amplitude dips sharply toward zero. Further, the magnitude of these steep time shifts decreases with frequency, as can be expected, since a careful measurement of the time shifts shows that they are approximately equal to one-half the period of the signal frequency. The explanation of this phenomenon is best understood in terms of discrete eigenray signals [9,10]. The eigenray signals, comprising the resultant received signal, may be represented as signal vectors in a complex phase-plane. The resultant signal vector is then the vector sum of all the signal vectors in the plane. At the point along the R axis where the acoustic field is near zero, the vector sum of the eigenray signals approaches the origin of the phase plane. In either direction from this range, the magnitude and phase of the resultant vector changes rapidly. However, the total phase shift in traversing through the null point will be limited to about $\pm \pi$ radians. When the resultant signal vector transitions clockwise through the null (as the range increases), the resultant time shift will be positive; if counterclockwise, the time shift will be negative (representing a decrease in the virtual propagation time). (Examples of the eigenray signal-vector approach to propagation analysis are given in Ref. 10.) A study of Figs. 2 through 10 reveals that the magnitude of the temporal fluctuations over the displayed range does not exceed $\pm$ 0.2 s, and it decreases with frequency for reasons given earlier.

(Text continues on page 13)

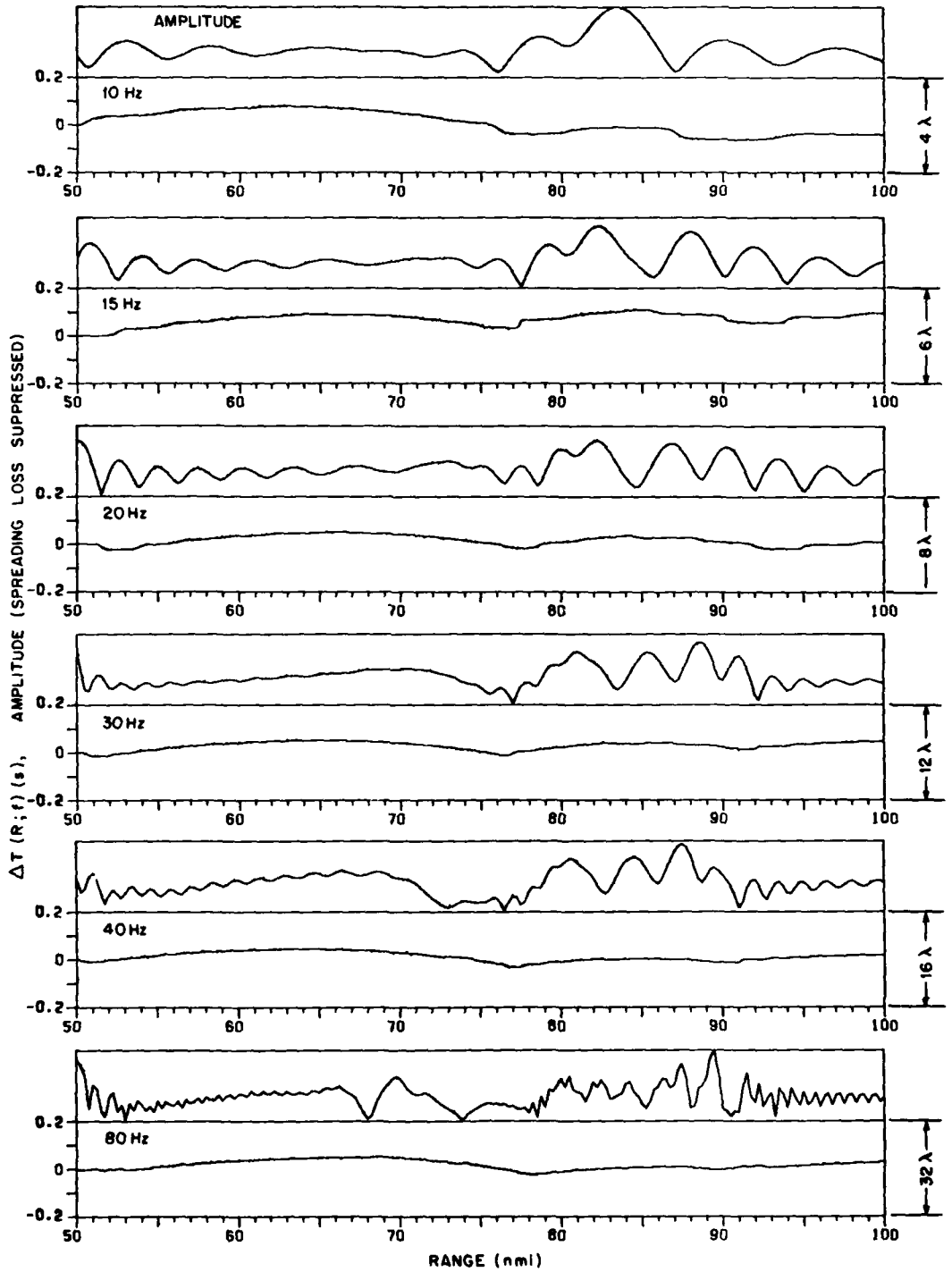

Fig. 2 — Fluctuations in virtual propagation time over the range 50 to 100 nmi for the six identified frequencies. The time fluctuations may be correlated with the normalized acoustic-field amplitude displayed over each time graph. For each signal frequency, the time scale in signal wave periods is shown at the right.

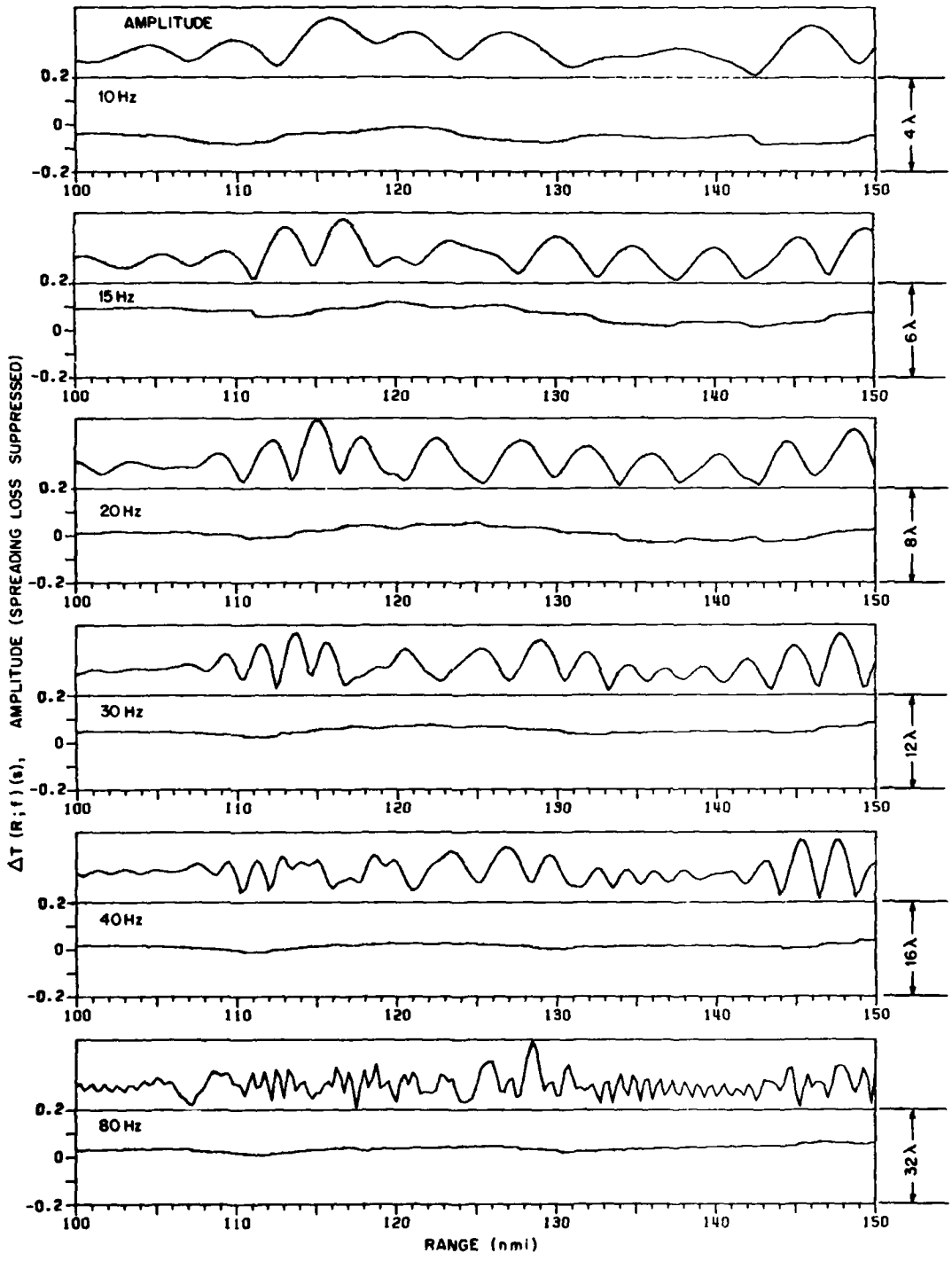

Fig. 3 — Fluctuations in virtual propagation time over the range 100 to 150 nmi for the six identified frequencies. The time fluctuations may be correlated with the normalized acoustic-field amplitude displayed over each time graph. For each signal frequency, the time scale in signal wave periods is shown at the right.

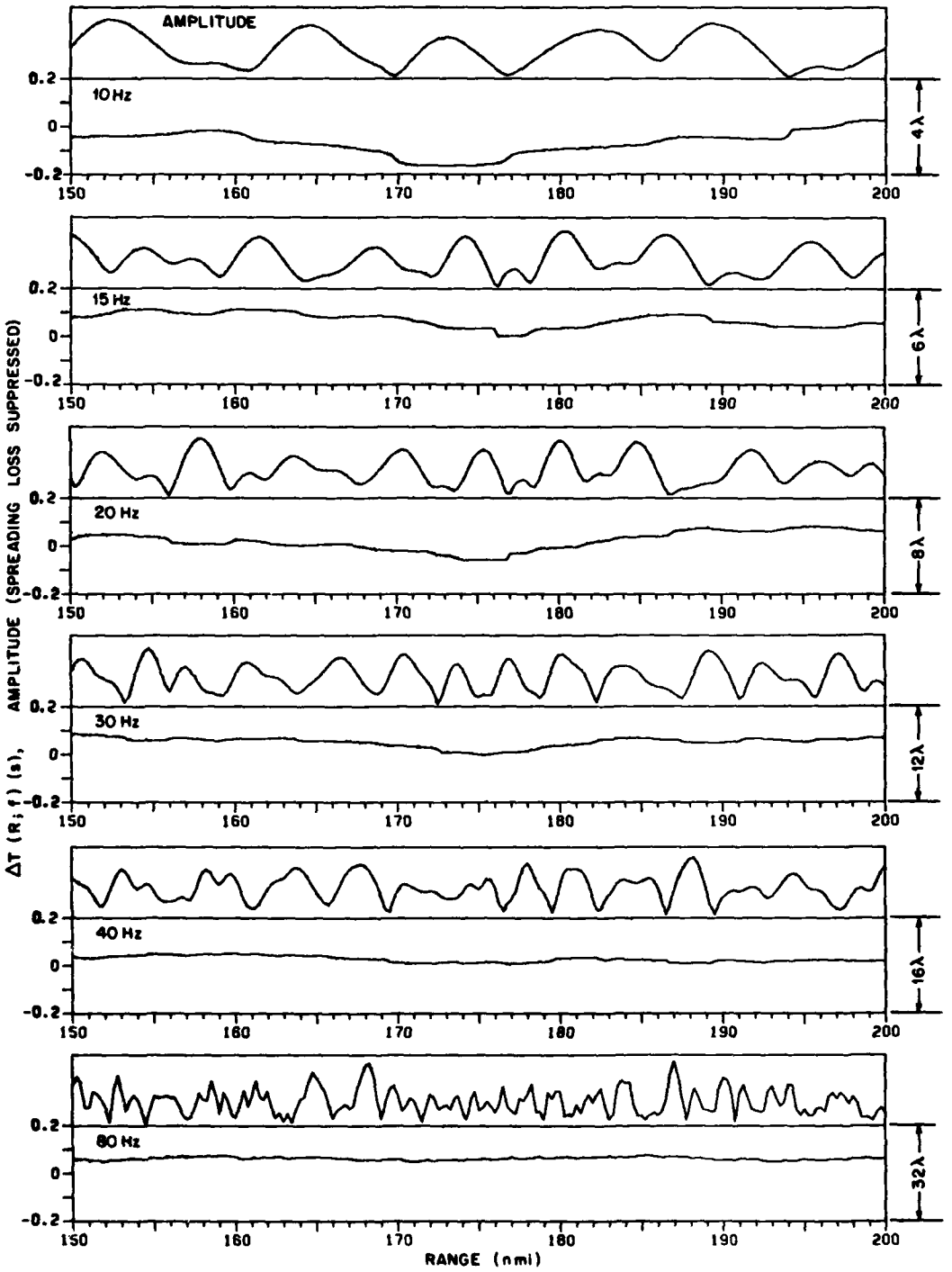

Fig. 4 — Fluctuations in virtual propagation time over the range 150 to 200 nmi for the six identified frequencies. The time fluctuations may be correlated with the normalized acoustic-field amplitude displayed over each time graph. For each signal frequency, the time scale in signal wave periods is shown at the right.

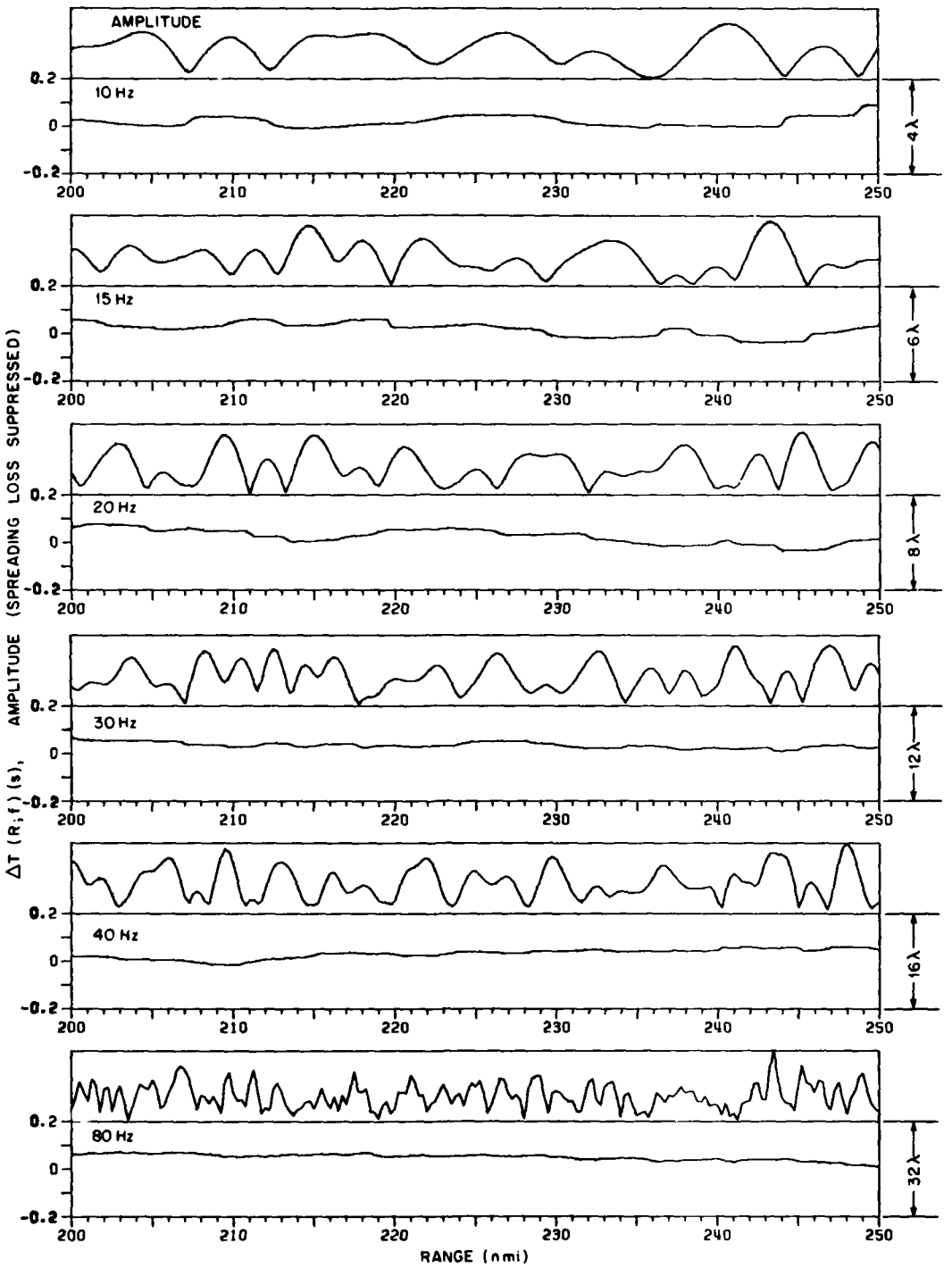

Fig. 5 — Fluctuations in virtual propagation time over the range 200 to 250 nmi for the six identified frequencies. The time fluctuations may be correlated with the normalized acoustic-field amplitude displayed over each time graph. For each signal frequency, the time scale in signal wave periods is shown at the right.

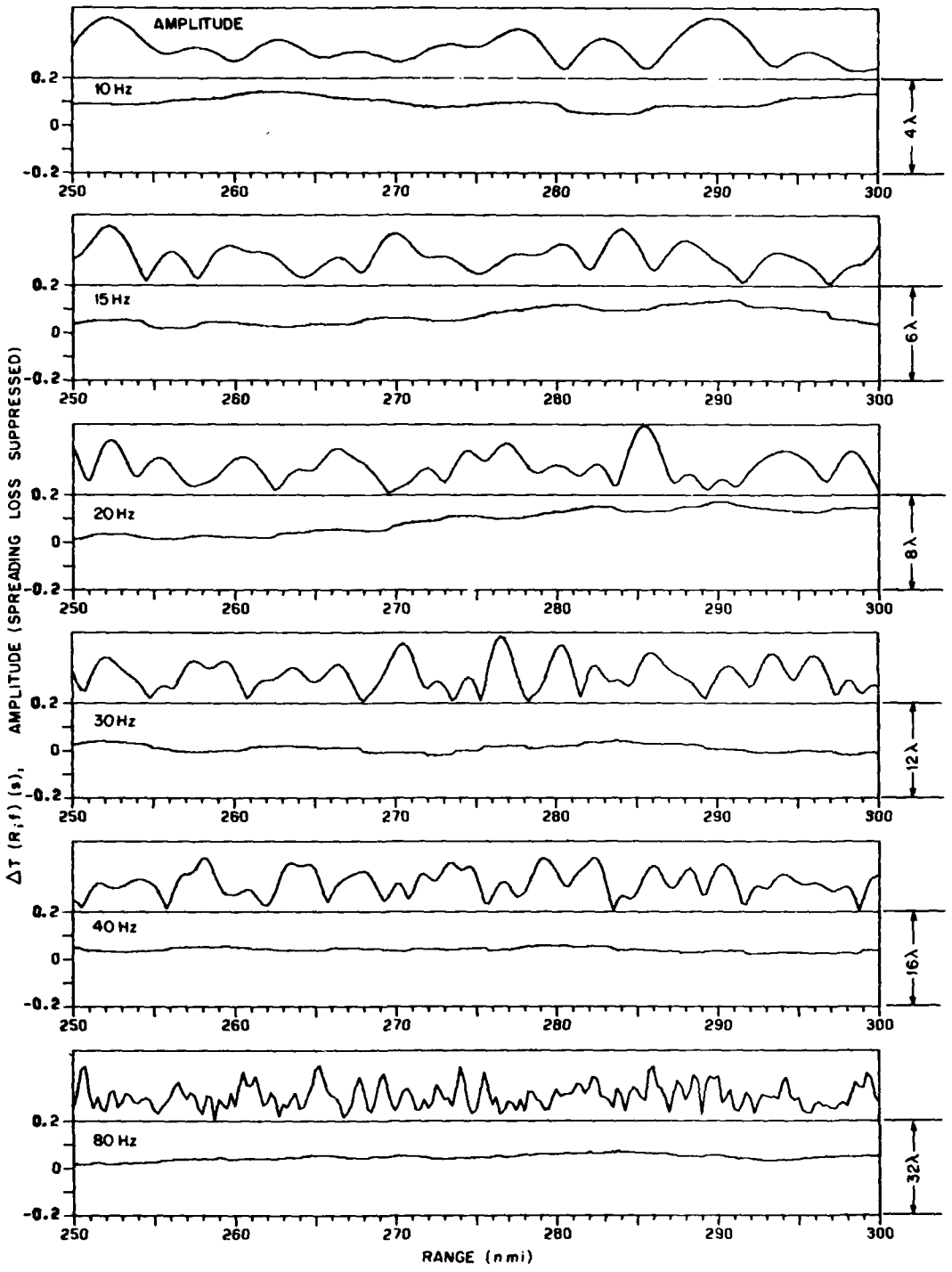

Fig. 6 — Fluctuations in virtual propagation time over the range 250 to 300 nmi for the six identified frequencies. The time fluctuations may be correlated with the normalized acoustic-field amplitude displayed over each time graph. For each signal frequency, the time scale in signal wave periods is shown at the right.

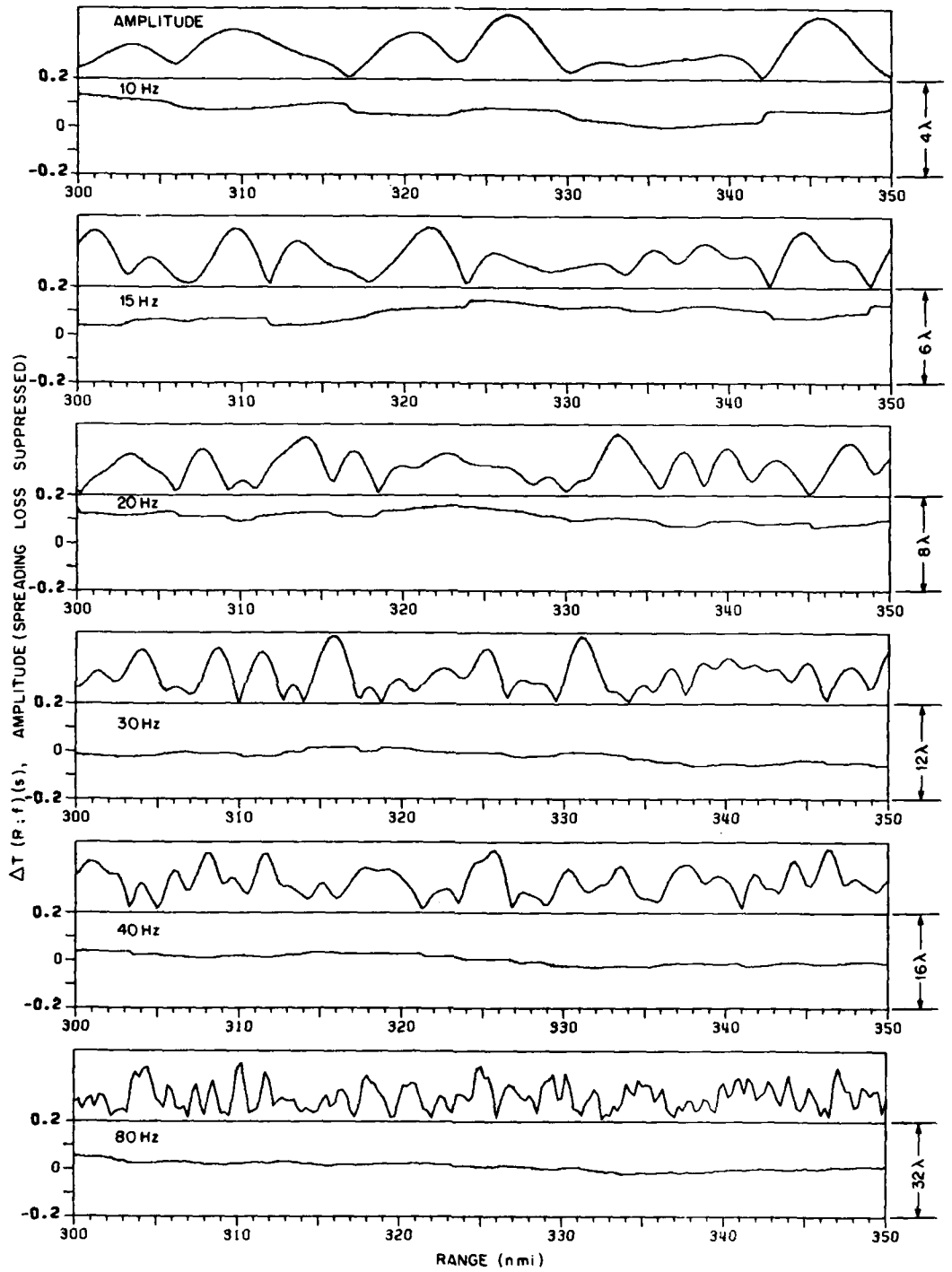

Fig. 7 — Fluctuations in virtual propagation time over the range 300 to 350 nmi for the six identified frequencies. The time fluctuations may be correlated with the normalized acoustic-field amplitude displayed over each time graph. For each signal frequency, the time scale in signal wave periods is shown at the right.

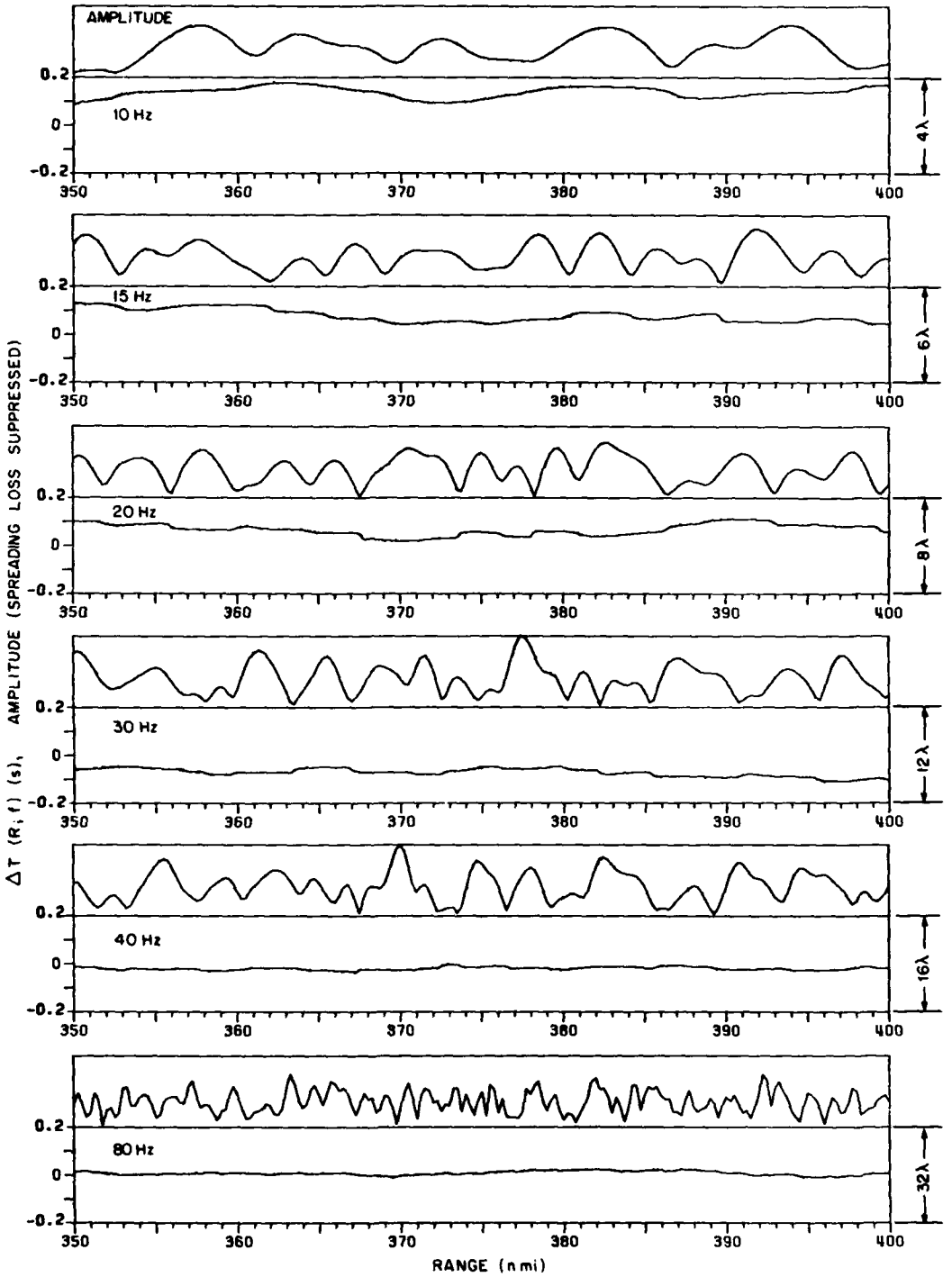

Fig. 8 — Fluctuations in virtual propagation time over the range 350 to 400 nmi for the six identified frequencies. The time fluctuations may be correlated with the normalized acoustic-field amplitude displayed over each time graph. For each signal frequency, the time scale in signal wave periods is shown at the right.

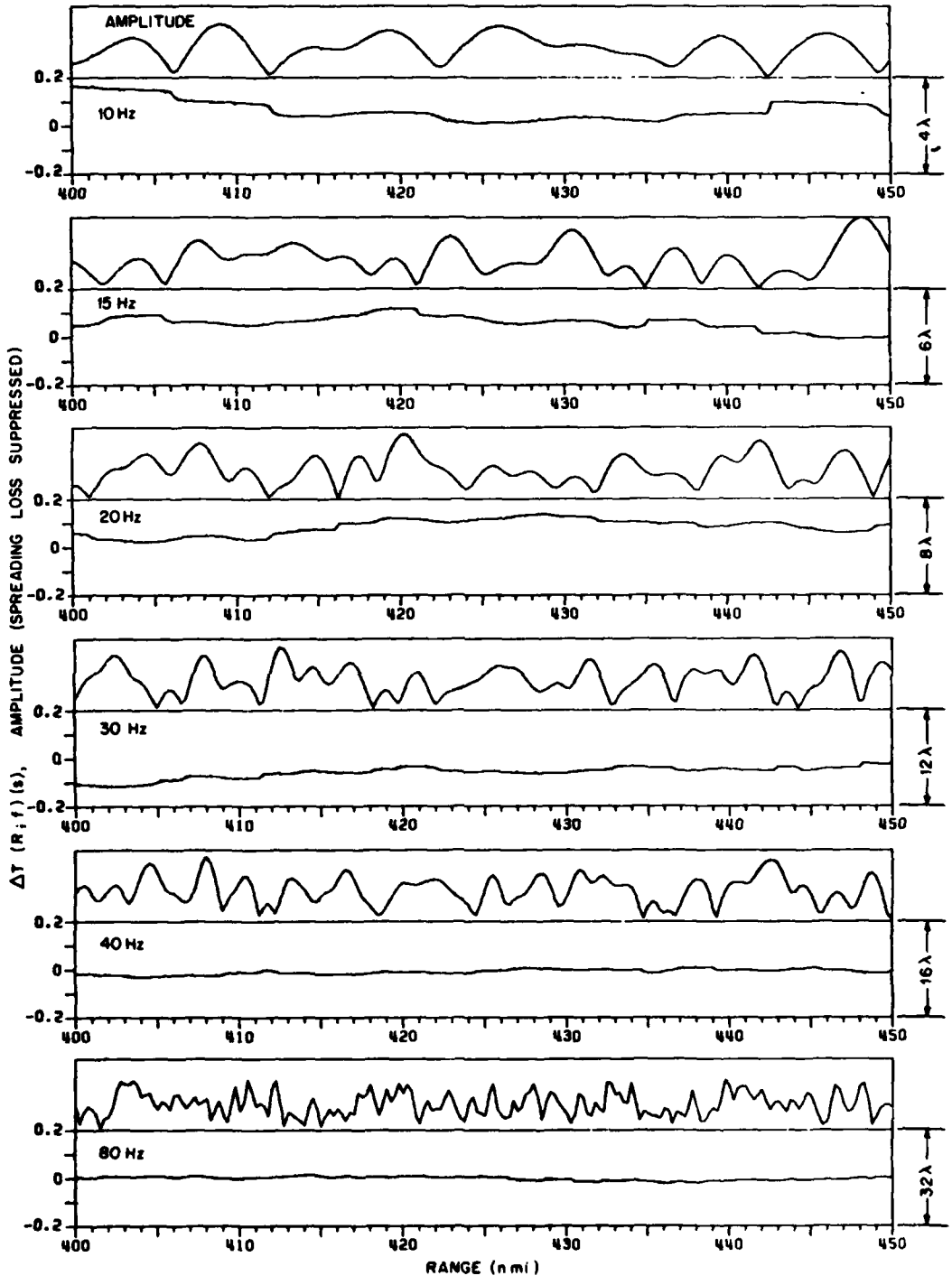

Fig. 9 — Fluctuations in virtual propagation time over the range 400 to 450 nmi for the six identified frequencies. The time fluctuations may be correlated with the normalized acoustic-field amplitude displayed over each time graph. For each signal frequency, the time scale in signal wave periods is shown at the right.

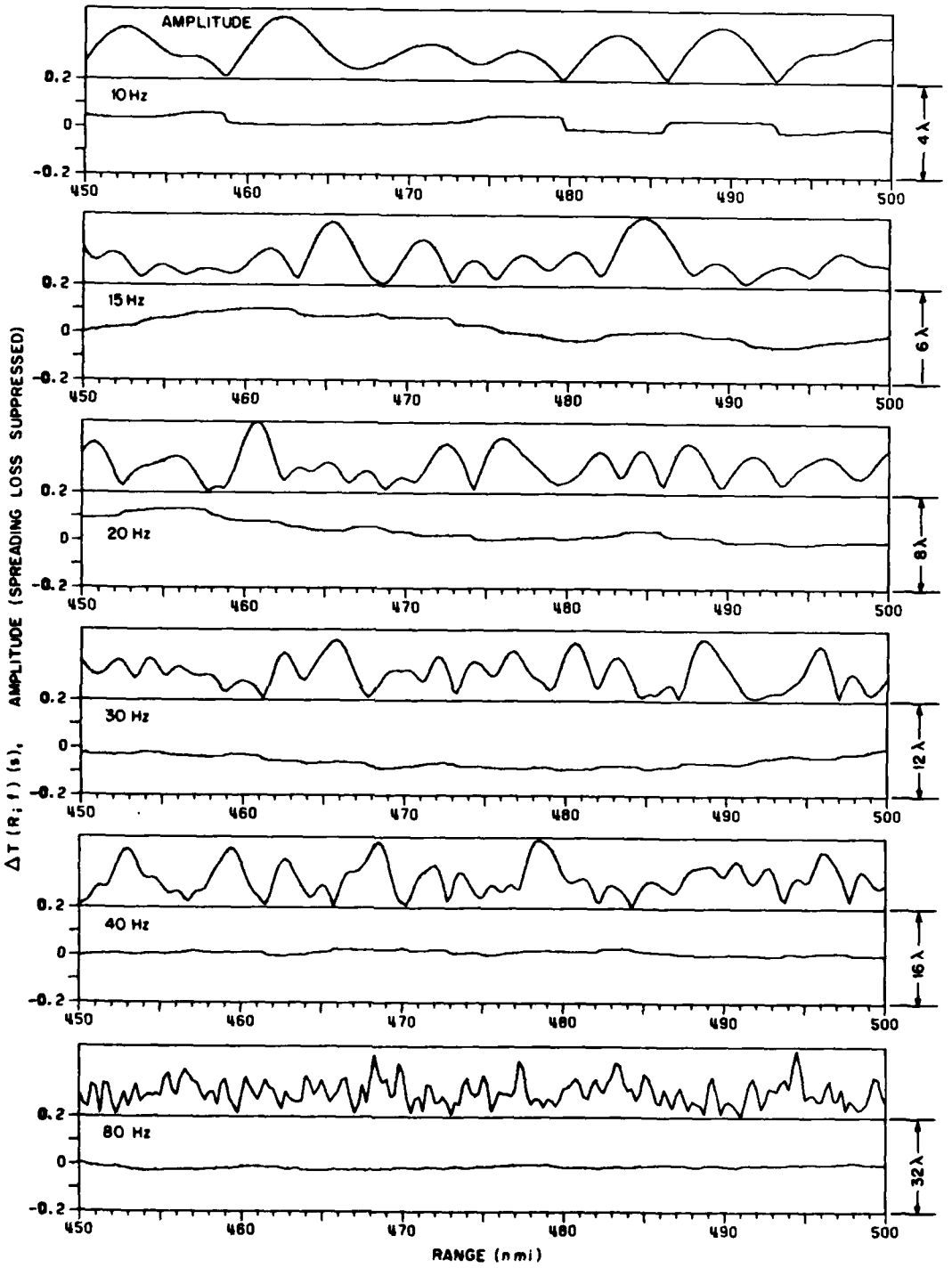

Fig. 10 — Fluctuations in virtual propagation time over the range 450 to 500 nmi for the six identified frequencies. The time fluctuations may be correlated with the normalized acoustic-field amplitude displayed over each time graph. For each signal frequency, the time scale in signal wave periods is shown at the right.

SPECTRAL DIFFERENCE IN PROPAGATION TIME

To study the difference in virtual propagation times between signals of different frequency, the following relation will be defined. Let

$$\tau(R_n;f_1,f_2) = T(R_n;f_2) - T(R_n;f_1)$$
$$= \frac{1}{2\pi f_2} \sum_{j=1}^{n} \left[\Delta\phi_{2,j} - q\Delta\phi_{1,j}\right], \quad (6)$$

where q is the signal-frequency ratio f_2/f_1, and the subscripts on the $\Delta\phi$s represent the computed phase differences for the two signals as given in Eq. (2). This spectral difference in propagation time has been computed over the range 50 to 500 nmi for 15 combinations of the frequencies considered earlier. The results are illustrated in Figs. 11 through 25.

Each figure displays the difference in propagation time over the range of 50 to 500 nmi for a given frequency pair. Over the range of 50 to 500 nmi, and for all frequency pairs, the difference in virtual propagation time is within ± 1.5 s. The peak-to-peak fluctuations in propagation time, for the individual pairs over this range, vary from about 1.4 s to less than 0.2 s. The mean peak-to-peak fluctuation is about 0.8 s over the range and for the frequency pairs tested.

From a study of the graphs, one may interpret the magnitude of the propagation-time fluctuations in terms of the phase fluctuation. On each figure, the equivalent wave periods (referenced to the higher of the two signal frequencies) of the 0.4-s time scale are marked on the right of the center scale. Thus, the phase fluctuation for a given time fluctuation will be proportional to the higher of the two signal frequencies, as demonstrated in Eq. (6).

(Text continues on page 29)

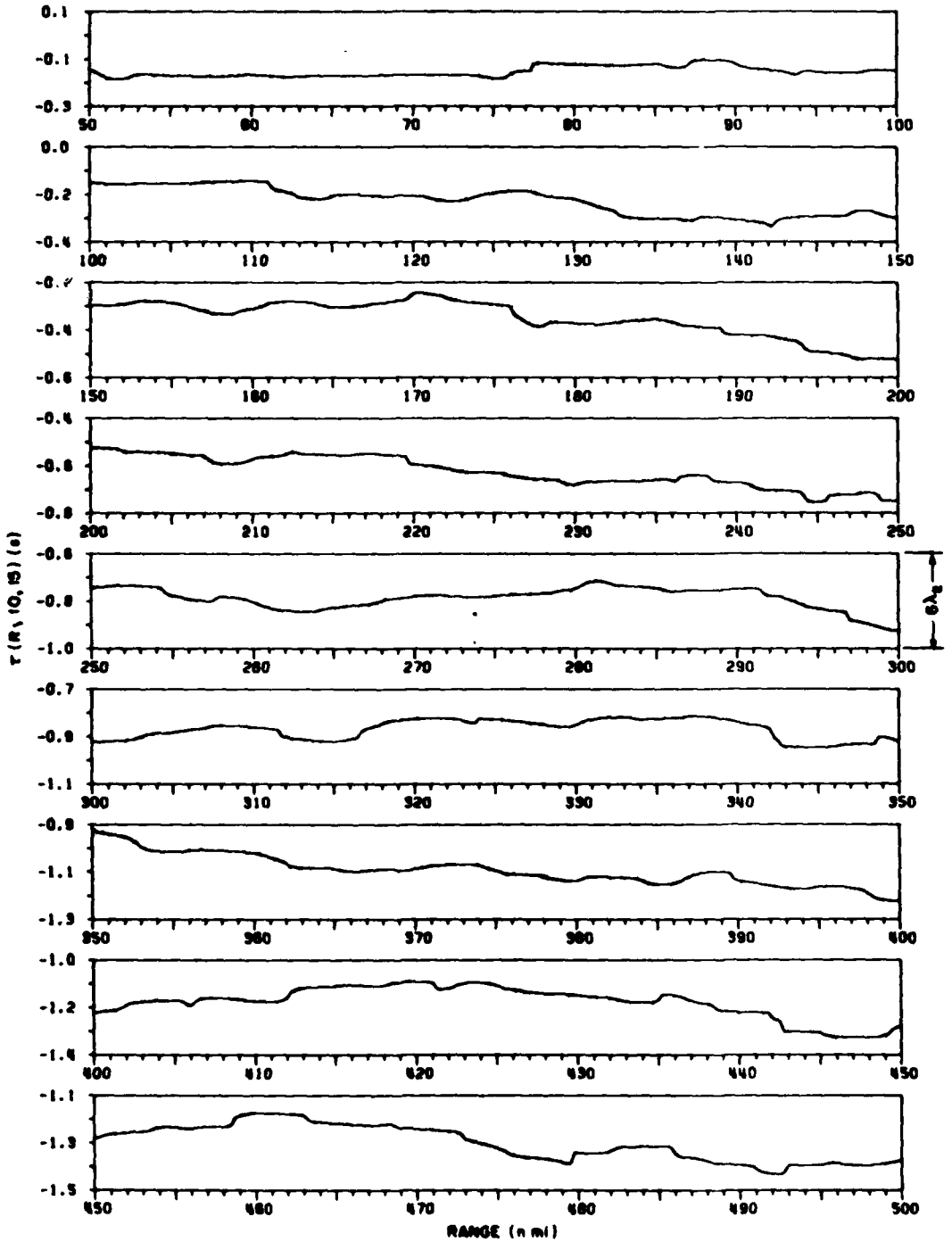

Fig. 11 — Difference in virtual propagation time, over the range 50 to 500 nmi, between sinusoidal signals of 10 and 15 Hz. The time scale, in wave periods of the upper frequency, is shown at the right of the center graph.

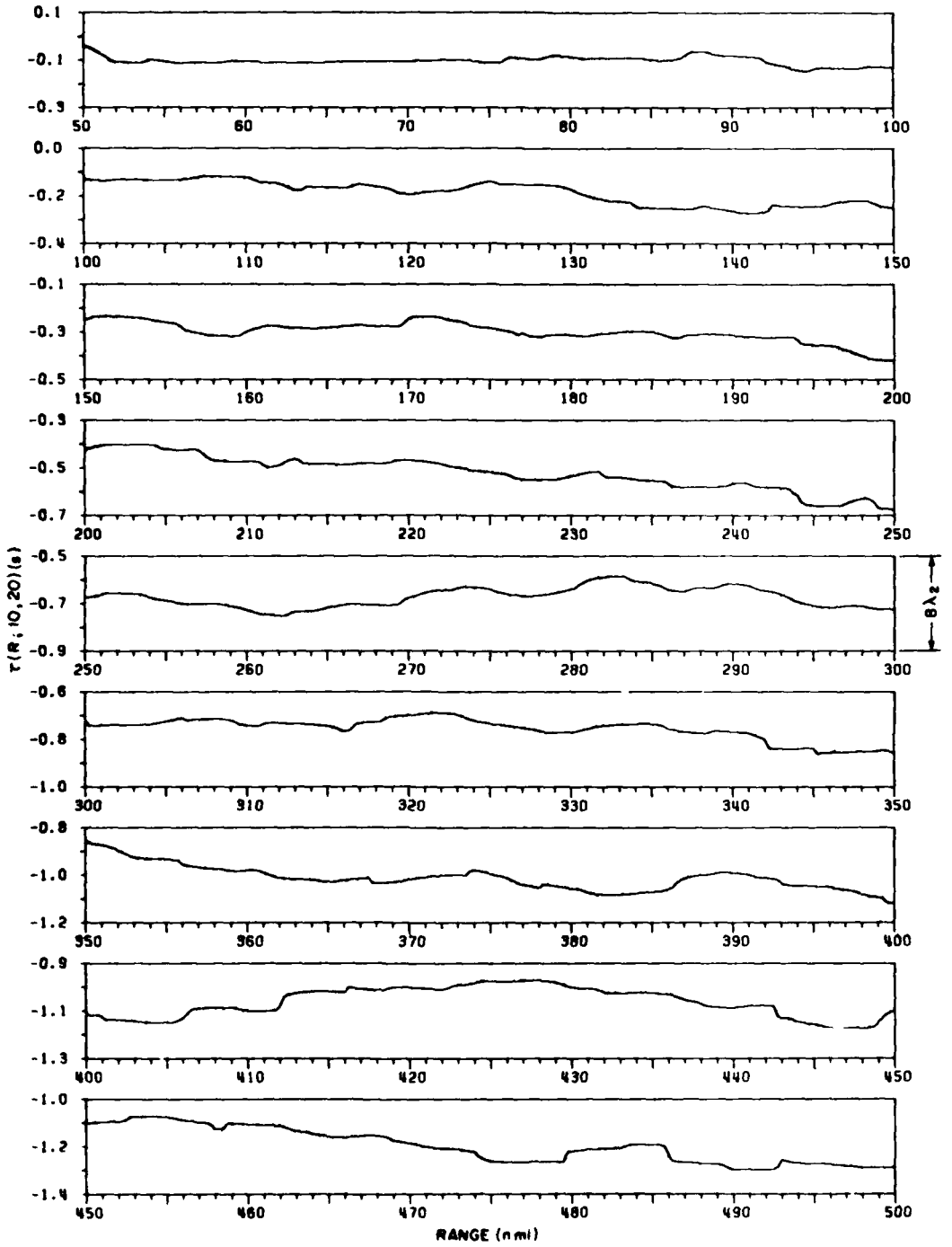

Fig. 12 — Difference in virtual propagation time, over the range 50 to 500 nmi, between sinusoidal signals of 10 and 20 Hz. The time scale, in wave periods of the upper frequency, is shown at the right of the center graph.

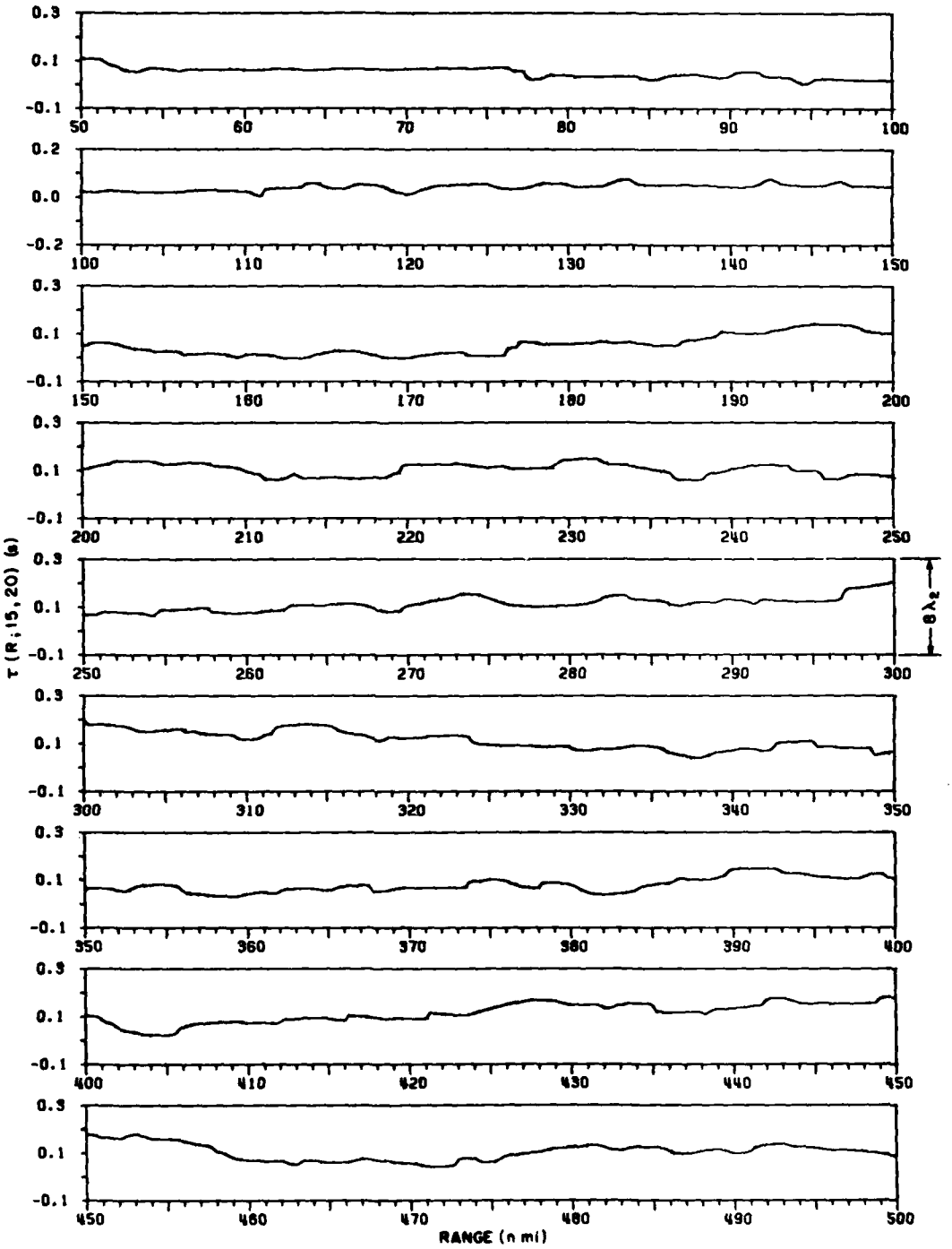

Fig. 13 — Difference in virtual propagation time, over the range 50 to 500 nmi, between sinusoidal signals of 15 and 20 Hz. The time scale, in wave periods of the upper frequency, is shown at the right of the center graph.

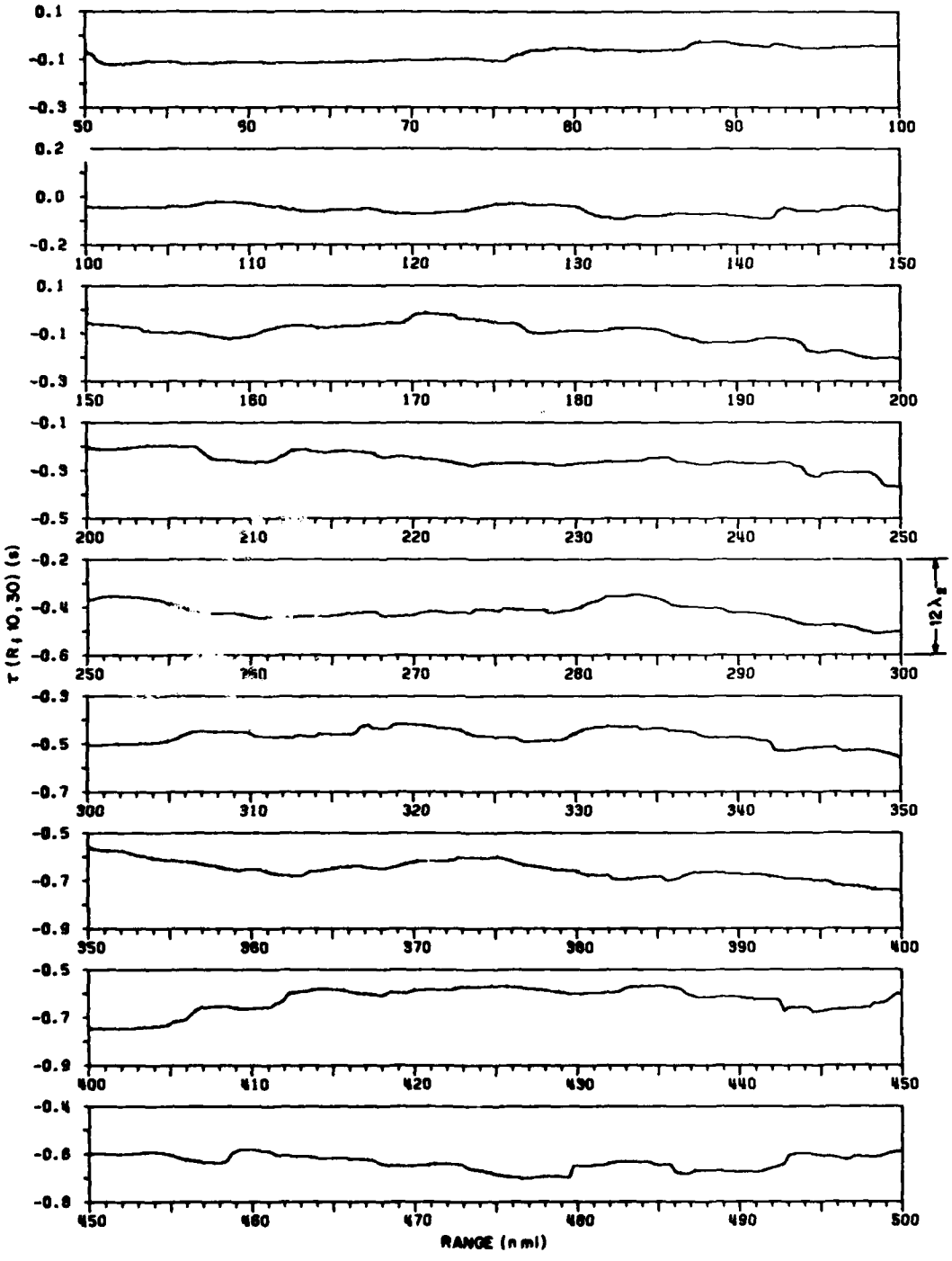

Fig. 14 — Difference in virtual propagation time, over the range 50 to 500 nmi, between sinusoidal signals of 10 and 30 Hz. The time scale, in wave periods of the upper frequency, is shown at the right of the center graph.

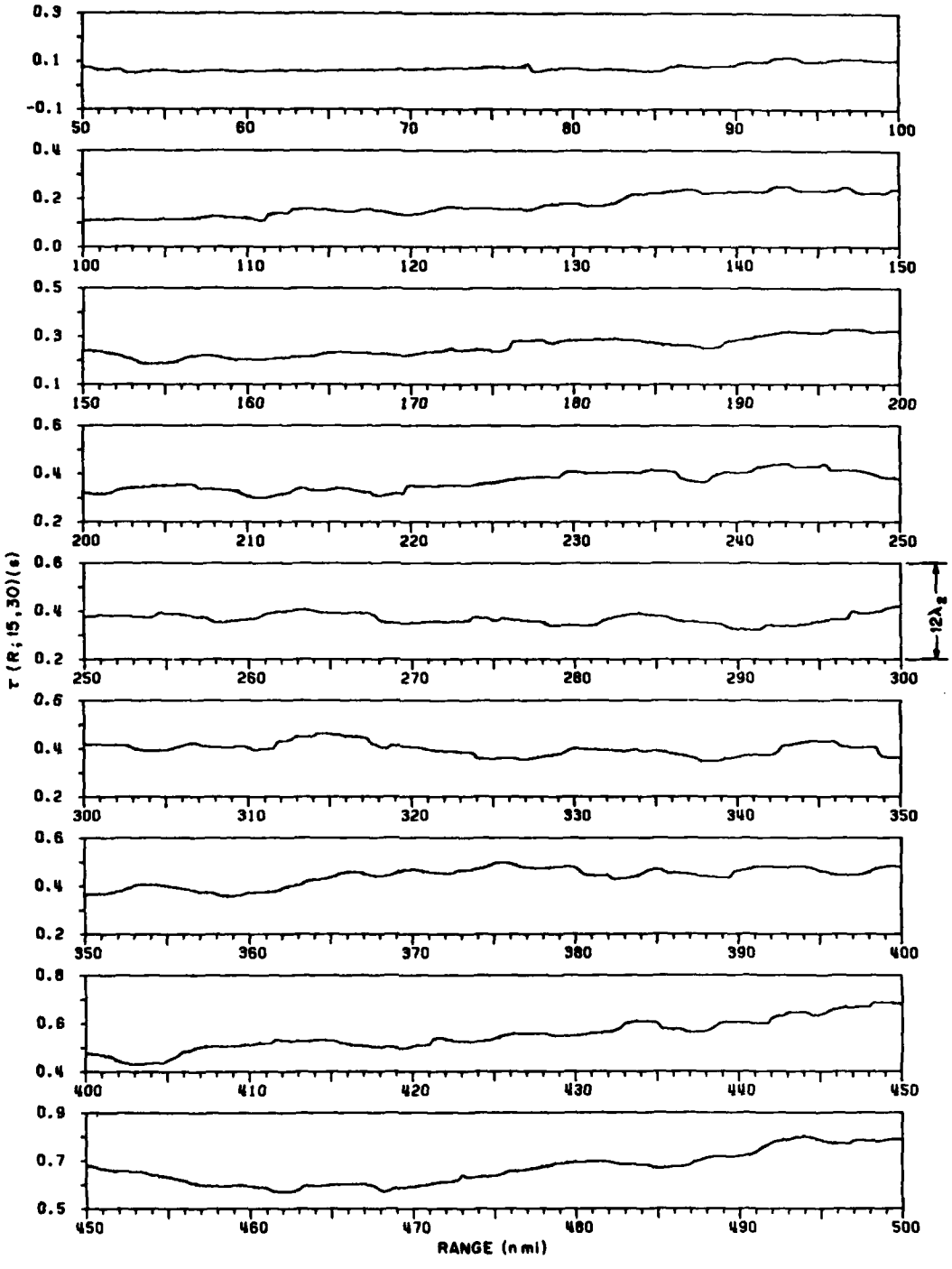

Fig. 15 — Difference in virtual propagation time, over the range 50 to 500 nmi, between sinusoidal signals of 15 and 30 Hz. The time scale, in wave periods of the upper frequency, is shown at the right of the center graph.

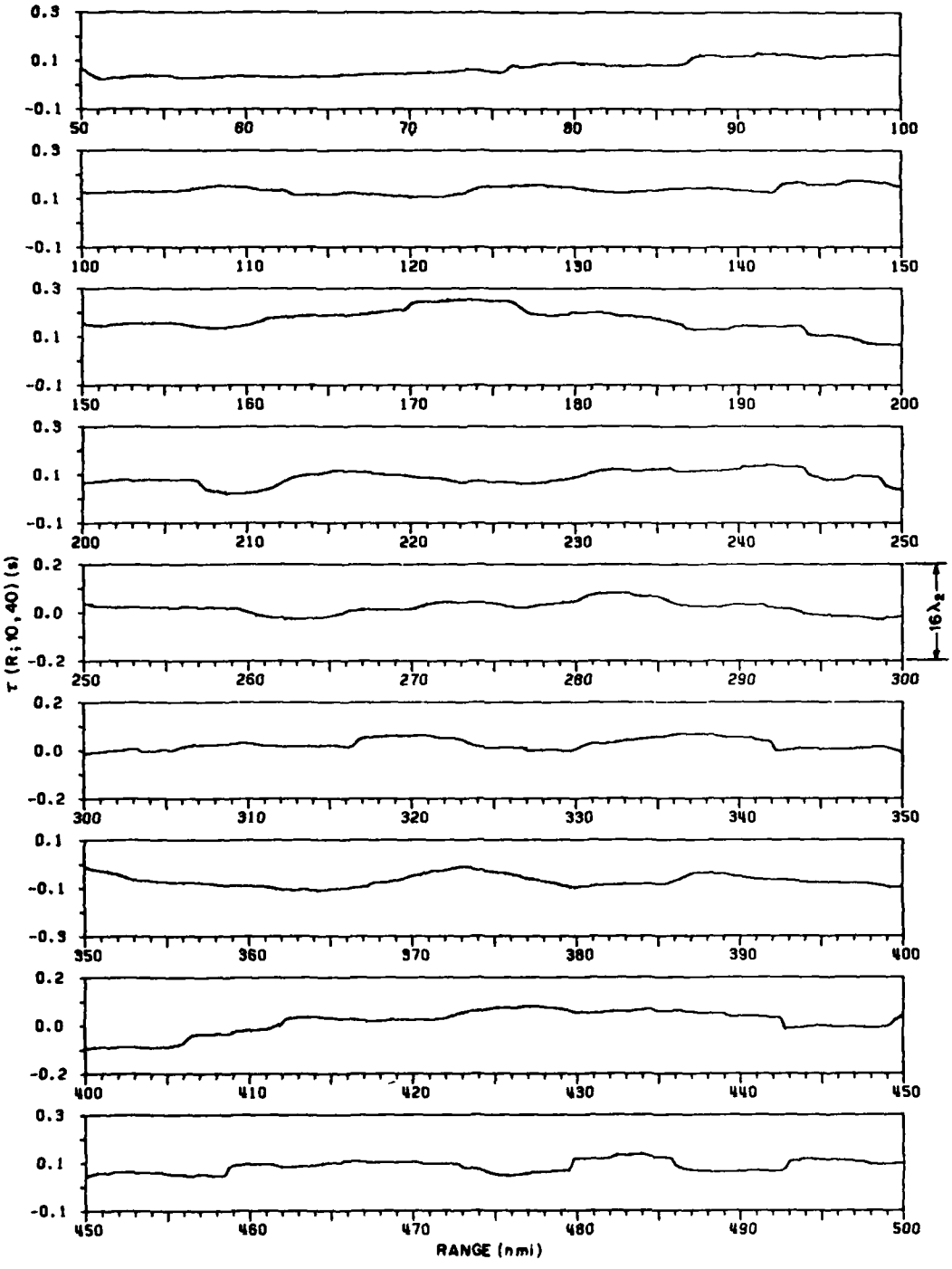

Fig. 16 — Difference in virtual propagation time, over the range 50 to 500 nmi, between sinusoidal signals of 10 and 40 Hz. The time scale, in wave periods of the upper frequency, is shown at the right of the center graph.

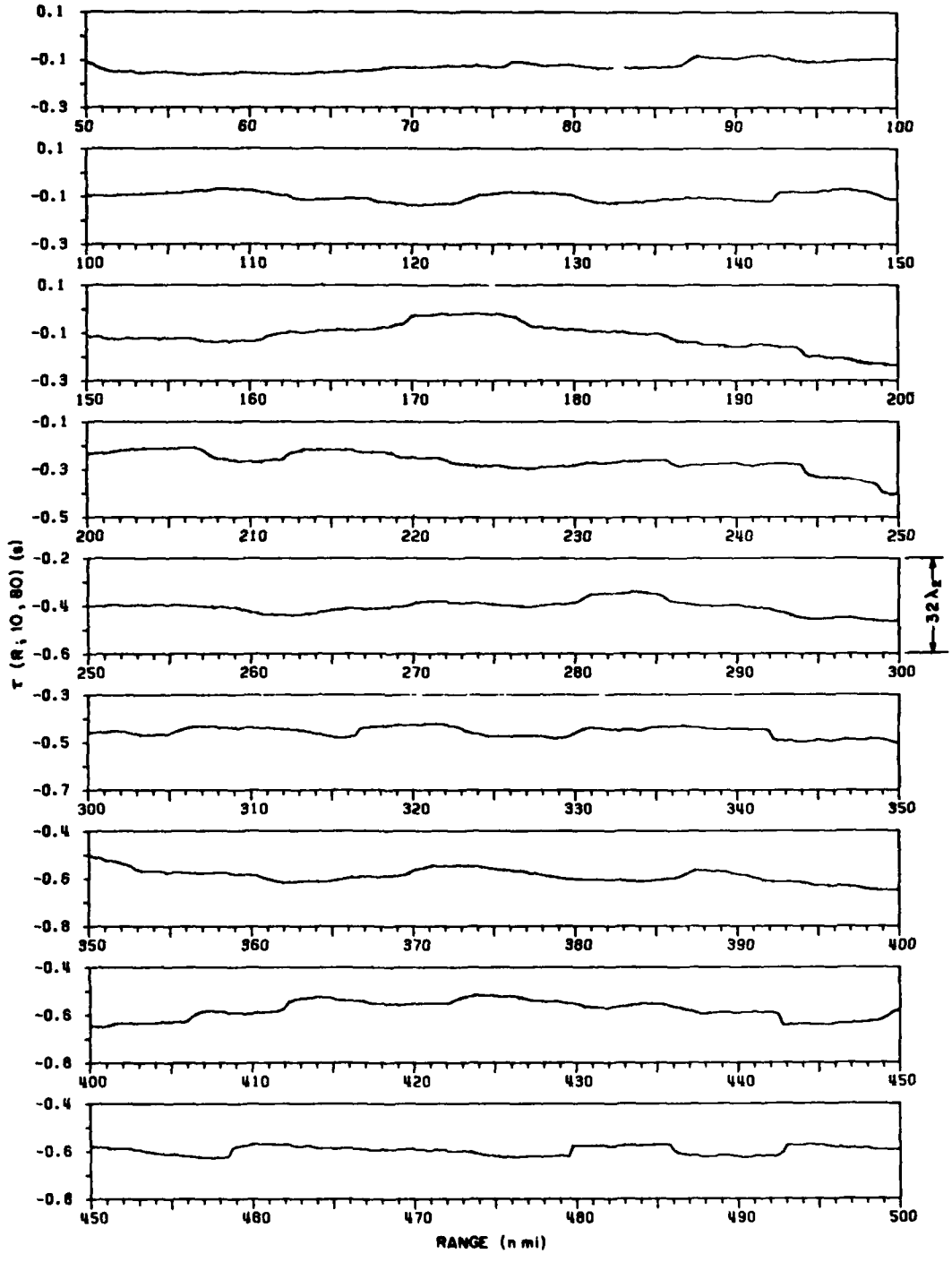

Fig. 17 — Difference in virtual propagation time, over the range 50 to 500 nmi, between sinusoidal signals of 10 and 80 Hz. The time scale, in wave periods of the upper frequency, is shown at the right of the center graph.

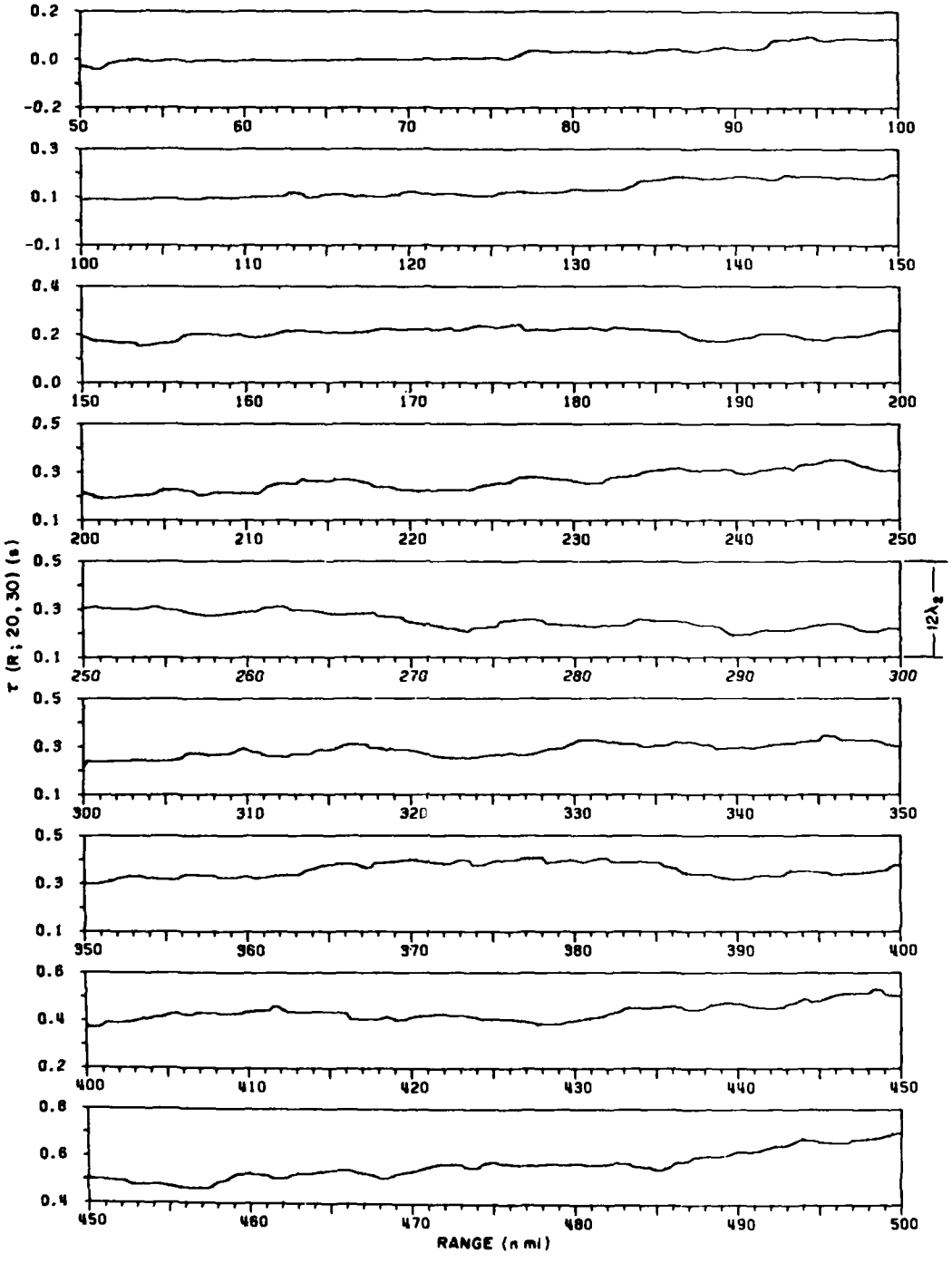

Fig. 18 — Difference in virtual propagation time, over the range 50 to 500 nmi, between sinusoidal signals of 20 and 30 Hz. The time scale, in wave periods of the upper frequency, is shown at the right of the center graph.

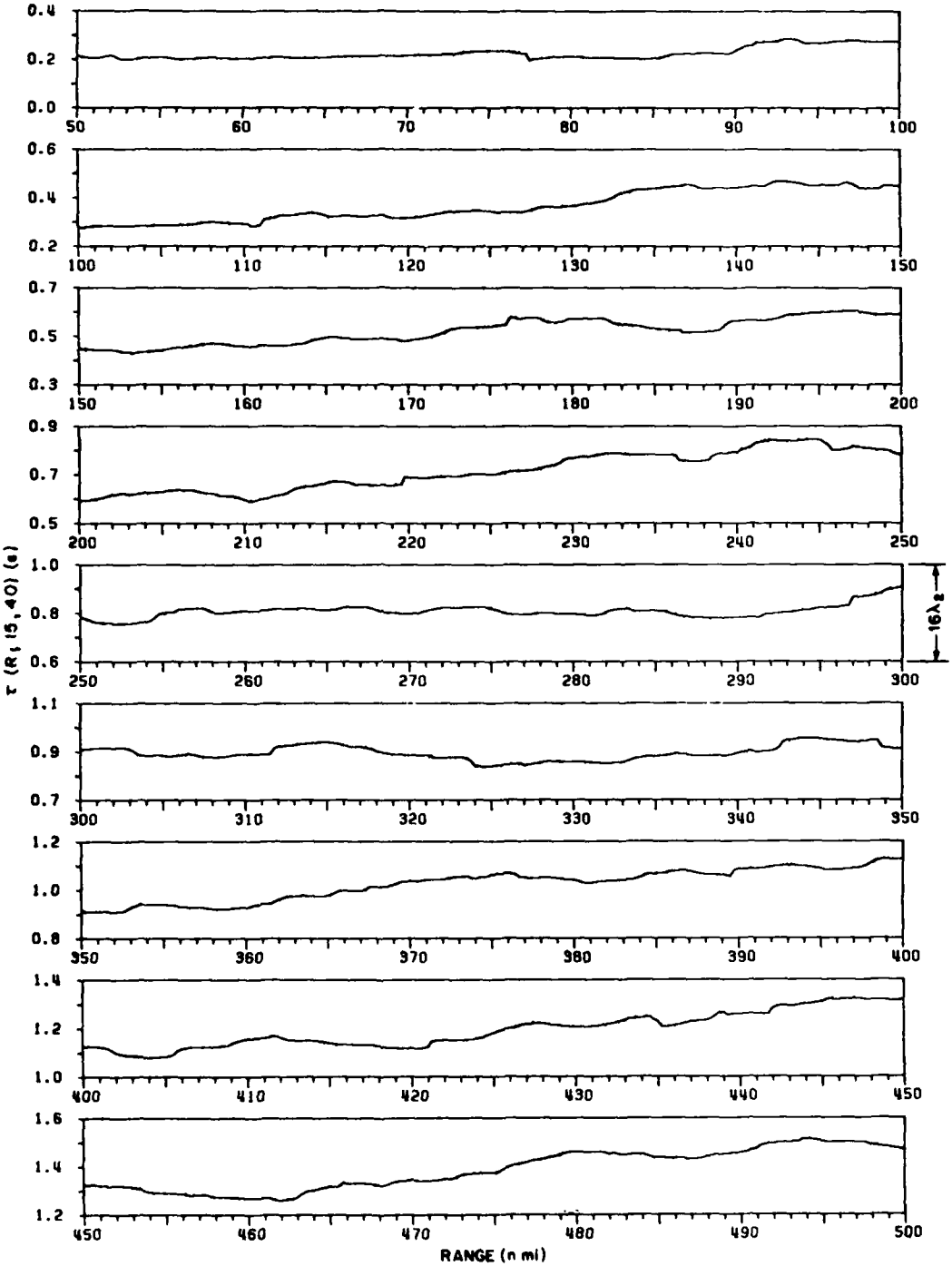

Fig. 19 — Difference in virtual propagation time, over the range 50 to 500 nmi, between sinusoidal signals of 15 and 40 Hz. The time scale, in wave periods of the upper frequency, is shown at the right of the center graph.

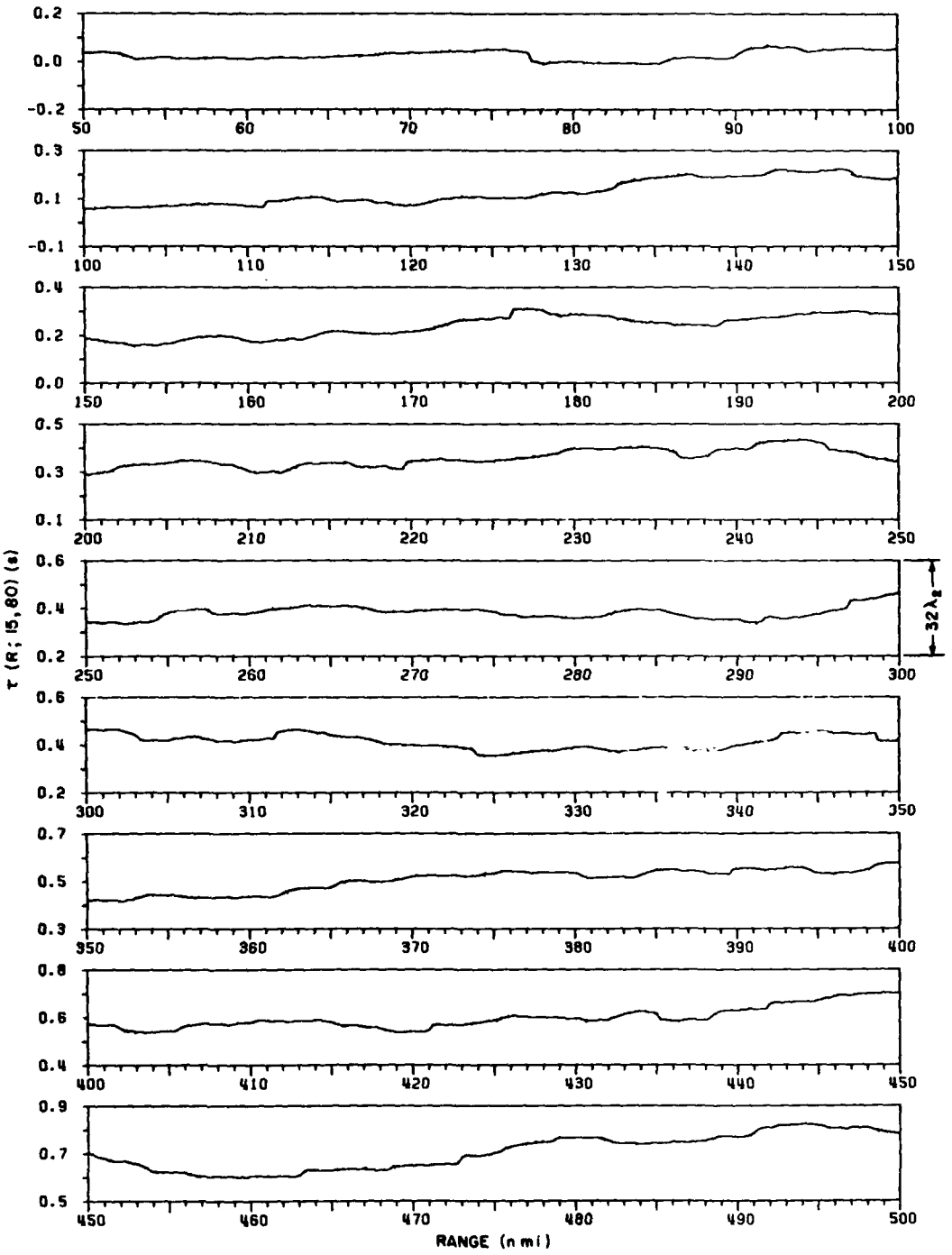

Fig. 20 — Difference in virtual propagation time, over the range 50 to 500 nmi, between sinusoidal signals of 15 and 80 Hz. The time scale, in wave periods of the upper frequency, is shown at the right of the center graph.

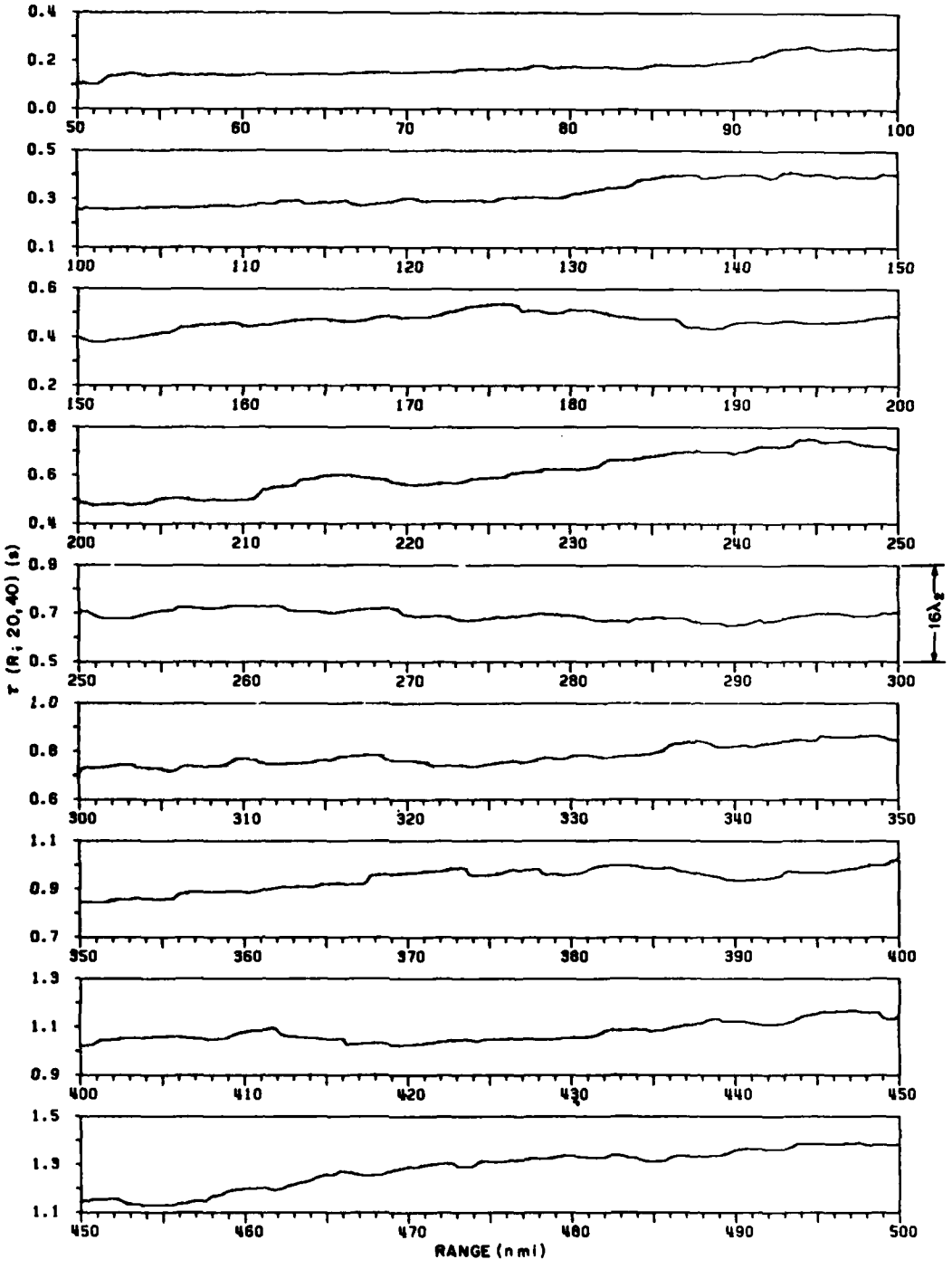

Fig. 21 — Difference in virtual propagation time, over the range 50 to 500 nmi, between sinusoidal signals of 20 and 40 Hz. The time scale, in wave periods of the upper frequency, is shown at the right of the center graph.

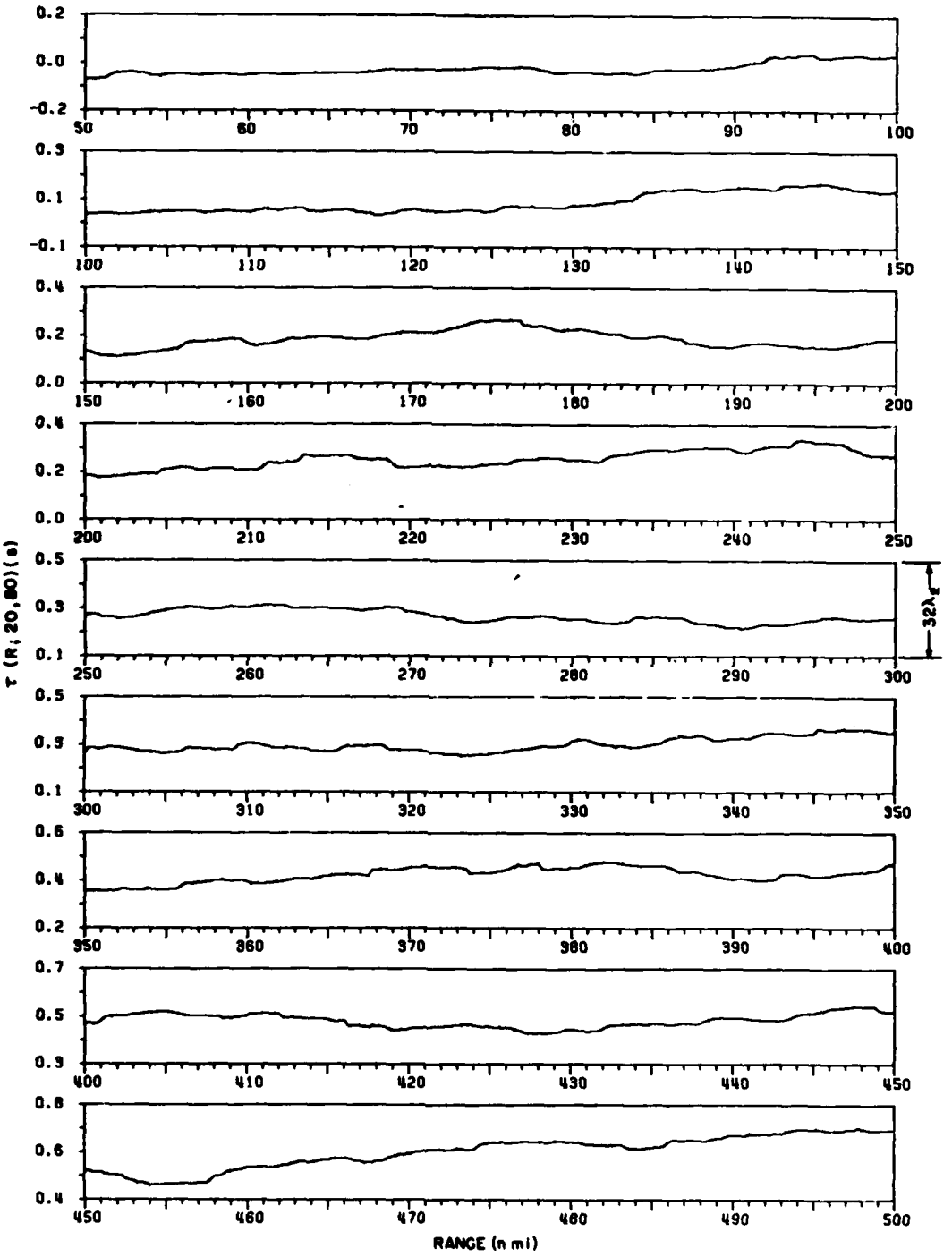

Fig. 22 — Difference in virtual propagation time, over the range 50 to 500 nmi, between sinusoidal signals of 20 and 80 Hz. The time scale, in wave periods of the upper frequency, is shown at the right of the center graph.

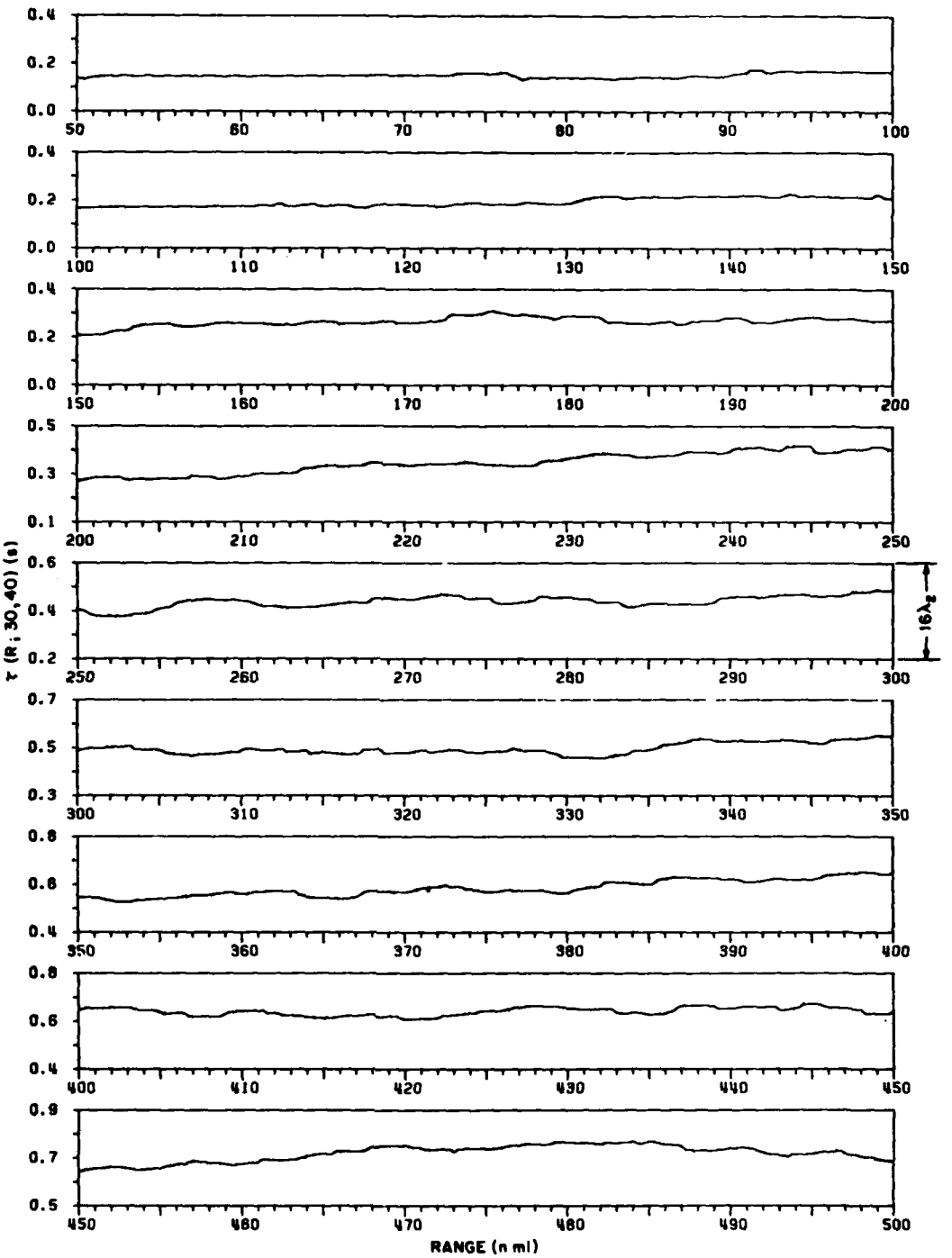

Fig. 23 — Difference in virtual propagation time, over the range 50 to 500 nmi, between sinusoidal signals of 30 and 40 Hz. The time scale, in wave periods of the upper frequency, is shown at the right of the center graph.

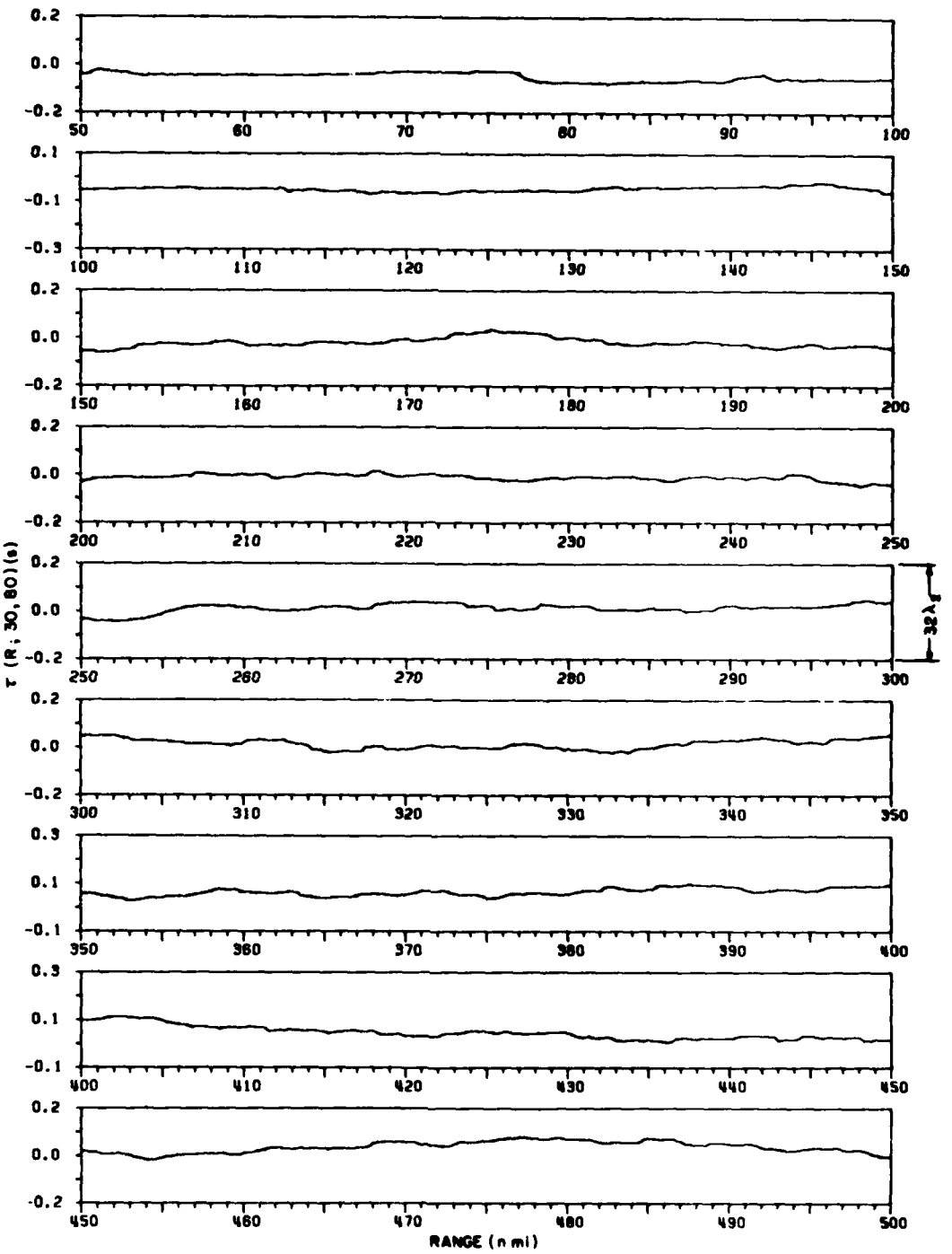

Fig. 24 — Difference in virtual propagation time, over the range 50 to 500 nmi, between sinusoidal signals of 30 and 80 Hz. The time scale, in wave periods of the upper frequency, is shown at the right of the center graph

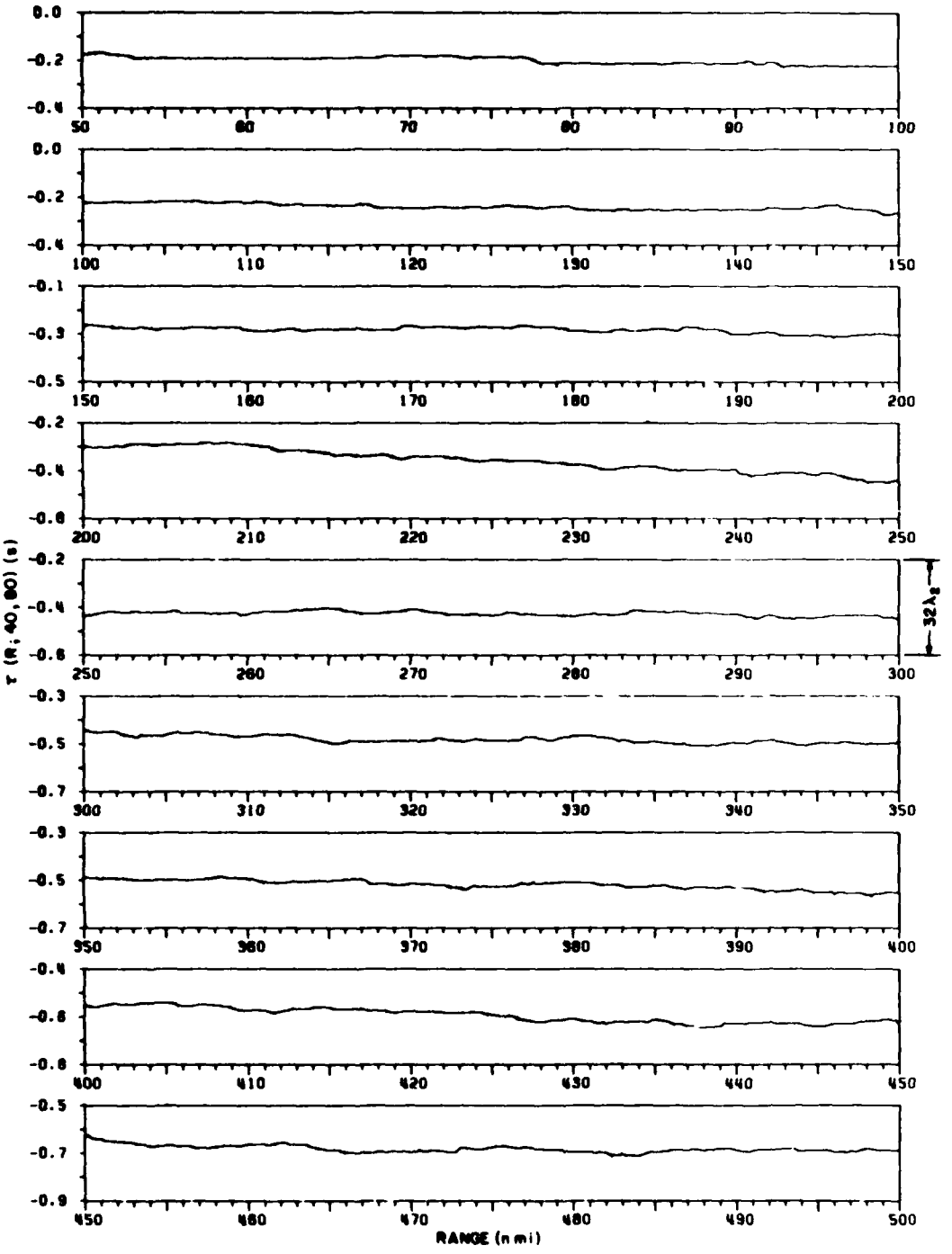

Fig. 25 — Difference in virtual propagation time, over the range 50 to 500 nmi, between sinusoidal signals of 40 and 80 Hz. The time scale, in wave periods of the upper frequency, is shown at the right of the center graph.

MEASURE OF SPECTRAL DISPERSION

In a dispersionless medium the value of $\tau(R_n;f_1,f_2)$ given by Eq. (6) would be zero over all R_n. The fact that this time difference varies with range is evidence of dispersion in the deep ocean channel. A useful measure of the frequency dispersion can be obtained if we consider a virtual frequency ratio $q'(R_n;f_1,f_2)$ which, when used in Eq. (6) in place of the actual frequency ratio q, will make $\tau(R_n;f_1,f_2)$ independent of range. The measure of the spectral dispersion will therefore be defined as the difference between the virtual and actual frequency ratios, or

$$\epsilon(R_n;f_1,f_2) = q'(R_n;f_1,f_2) - q. \tag{7}$$

To determine the error in frequency ratio, a dynamic variable is required to create a change in the variables with time. Consequently, the range variable R is parameterized to vary with time. In this circumstance, the observed frequencies f_1' and f_2' at the point R will be

$$f_2'(R;f_2) = f_2 - \frac{1}{2\pi}\dot{\phi}(R;f_2) = f_2[1 - \dot{T}(R;f_2)] \tag{8a}$$

and

$$f_1'(R;f_1) = f_1 - \frac{1}{2\pi}\dot{\phi}(R;f_1) = f_1[1 - \dot{T}(R;f_1)], \tag{8b}$$

where the dot over the variable implies the derivative with respect to time. The virtual frequency ratio is then the ratio of the observed (virtual) signal frequencies, or

$$q'(R;f_1,f_2) = q\frac{1 - \dot{T}(R;f_2)}{1 - \dot{T}(R;f_1)} \approx q[1 - \dot{\tau}(R;f_1,f_2)] \tag{9}$$

and

$$\epsilon(R;f_1,f_2) \approx -q\dot{\tau}(R;f_1,f_2) = -q\dot{R}\frac{d}{dR}\tau(R;f_1,f_2). \tag{10}$$

Thus, the measure of frequency dispersion is proportional to the product of the true frequency ratio q, the source-sensor range-rate $\dot{R}$ (in meters per second), and the slope of the function $\tau(R;f_1,f_2)$. In terms of the discrete measures of the variables,

$$\frac{\epsilon(R_n;f_1,f_2)}{q\dot{R}} = \frac{-0.515}{K}[\tau(R_n;f_1,f_2) - \tau(R_{n-1};f_1,f_2)], \tag{11}$$

where $\dot{R}$ is the range rate expressed in knots. The above function has been computed over the range of 50 to 500 nmi for the frequency combinations considered earlier. The results are illustrated in Figs. 26 through 40.

A study of the illustrations reveals that, except for the occasional sharp spikes along the range axis, the frequency dispersion is rather moderate. As may be conjectured, the sharp spikes occur at points where the virtual propagation time changes rapidly with range for either frequency. It will be noticed, too, that the peaks of the spikes are smaller when both signal frequencies are large. It is important to recall that the spikes are induced at ranges where the amplitude of either signal is exceptionally low (see Figs. 2 through 10). Thus, an experimental observation of their existence will be difficult to achieve in a noisy signal background. It may be concluded that they play a rather insignificant role in practical applications of underwater acoustics.

(Text continues on page 45)

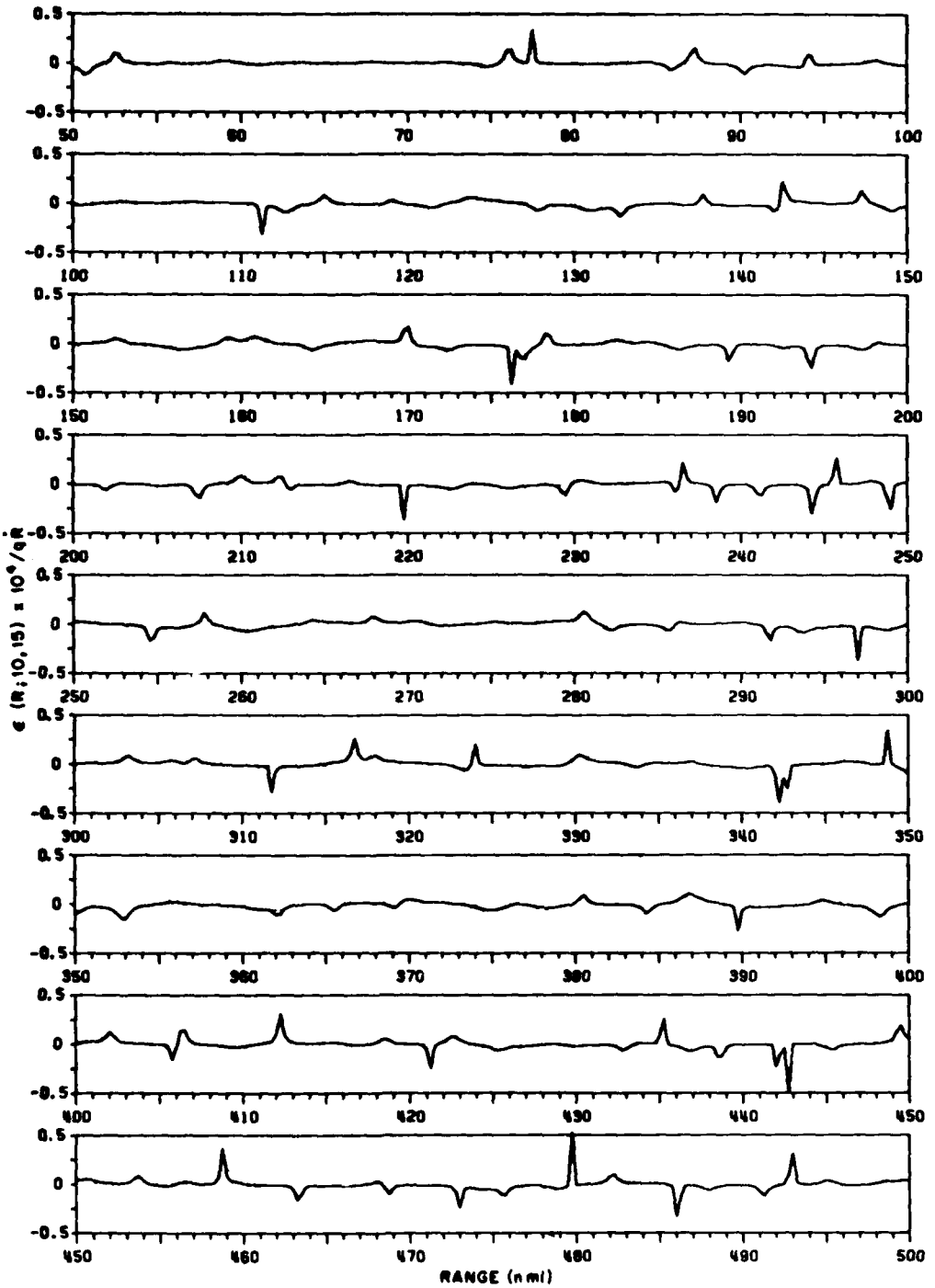

Fig. 26 — Dispersion measure $\epsilon \times 10^4 / qR$, over the range 50 to 500 nmi, between sinusoidal signals of 10 and 15 Hz. The measure of dispersion is the difference between the observed (or virtual) frequency ratio q' and the true frequency ratio q, R is the range rate in knots.

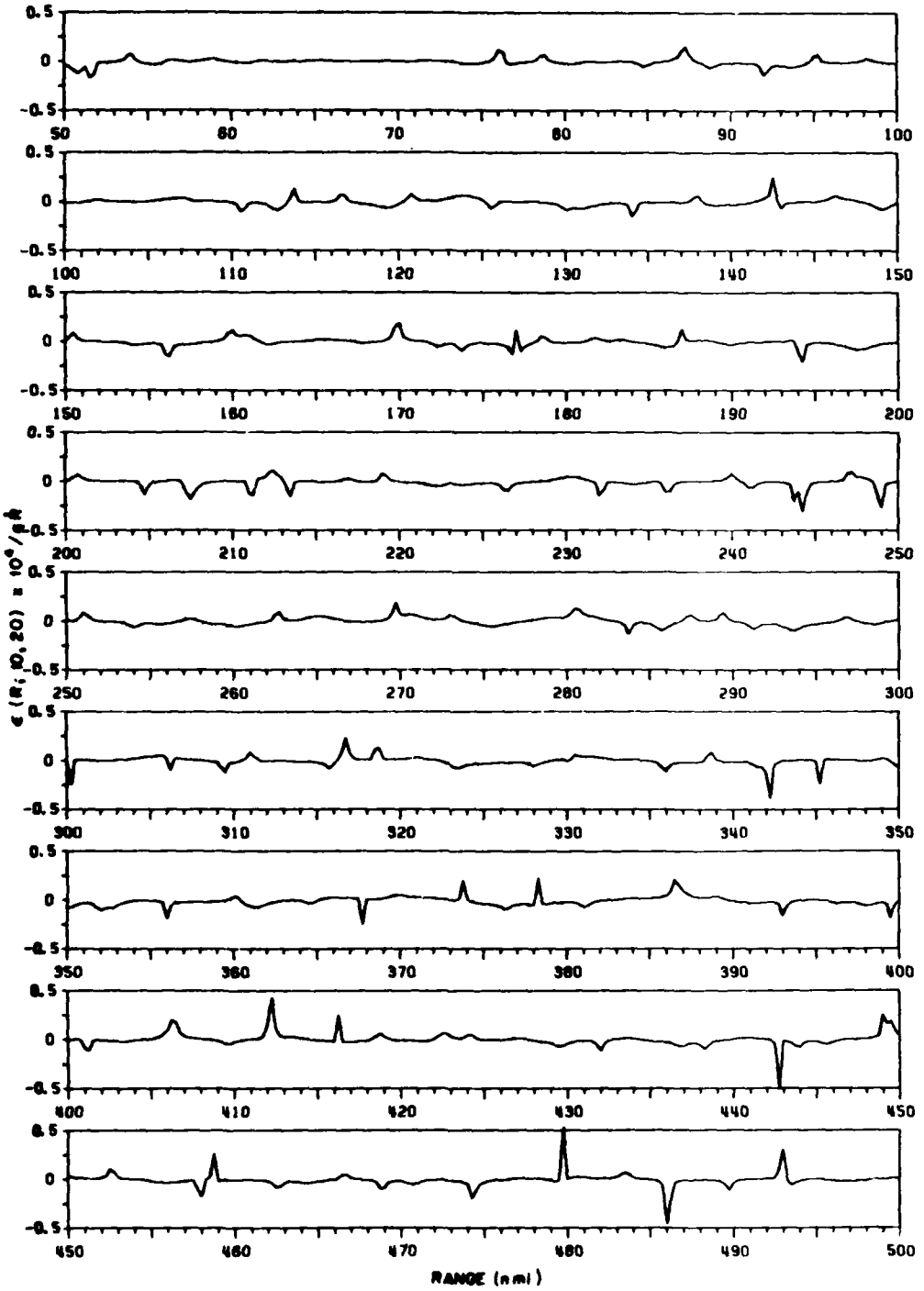

Fig. 27 — Dispersion measure $\epsilon \times 10^4 / qR$, over the range 50 to 500 nmi, between sinusoidal signals of 10 and 20 Hz. The measure of dispersion is the difference between the observed (or virtual) frequency ratio q' and the true frequency ratio q. R is the range rate in knots.

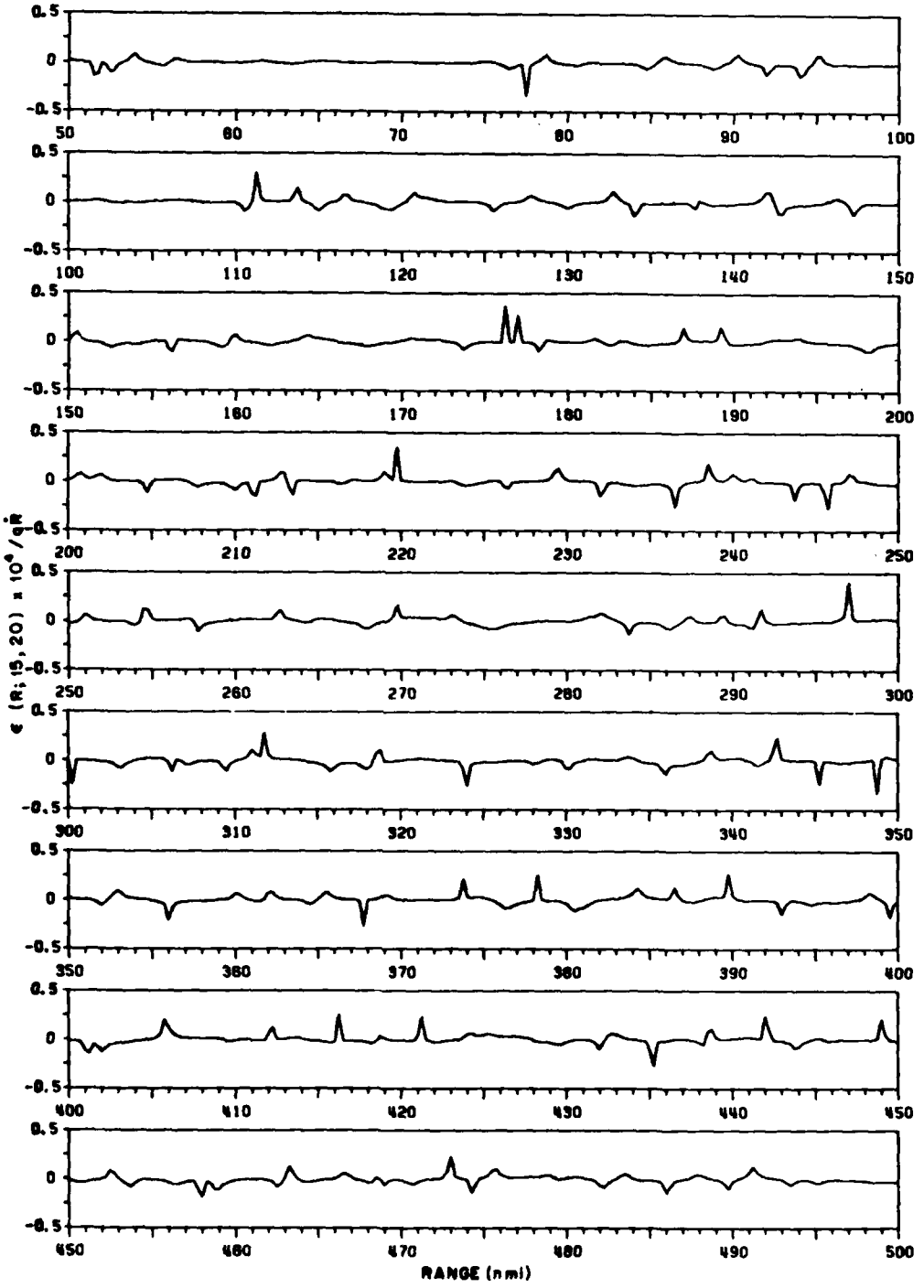

Fig. 28 — Dispersion measure $\epsilon \times 10^4 / \eta \dot{R}$, over the range 50 to 500 nmi, between sinusoidal signals of 15 and 20 Hz. The measure of dispersion is the difference between the observed (or virtual) frequency ratio q' and the true frequency ratio q, $\dot{R}$ is the range rate in knots.

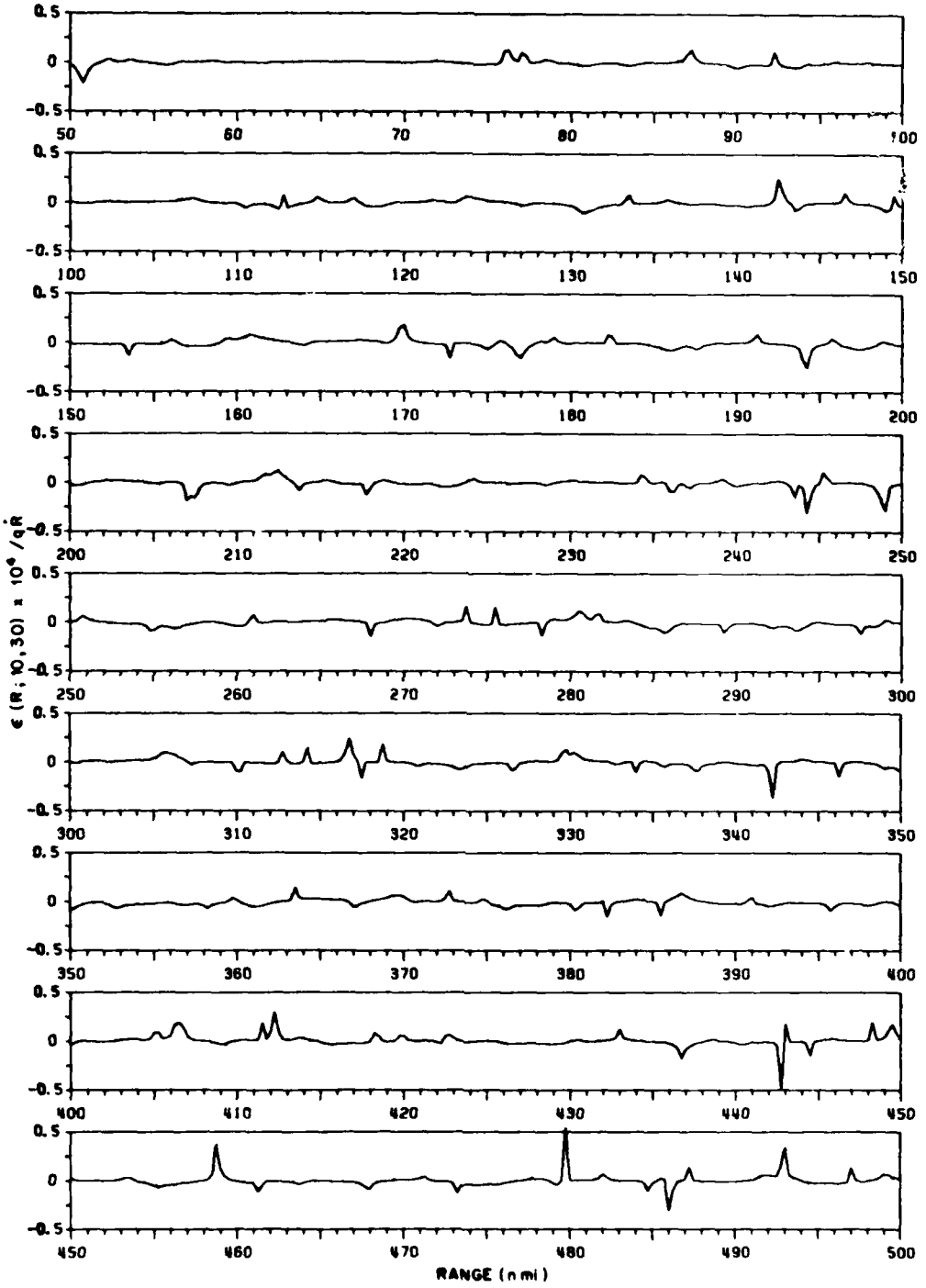

Fig. 29 — Dispersion measure $\epsilon \times 10^4 / qR$, over the range 50 to 500 nmi, between sinusoidal signals of 10 and 30 Hz. The measure of dispersion is the difference between the observed (or virtual) frequency ratio q' and the true frequency ratio q. R is the range rate in knots.

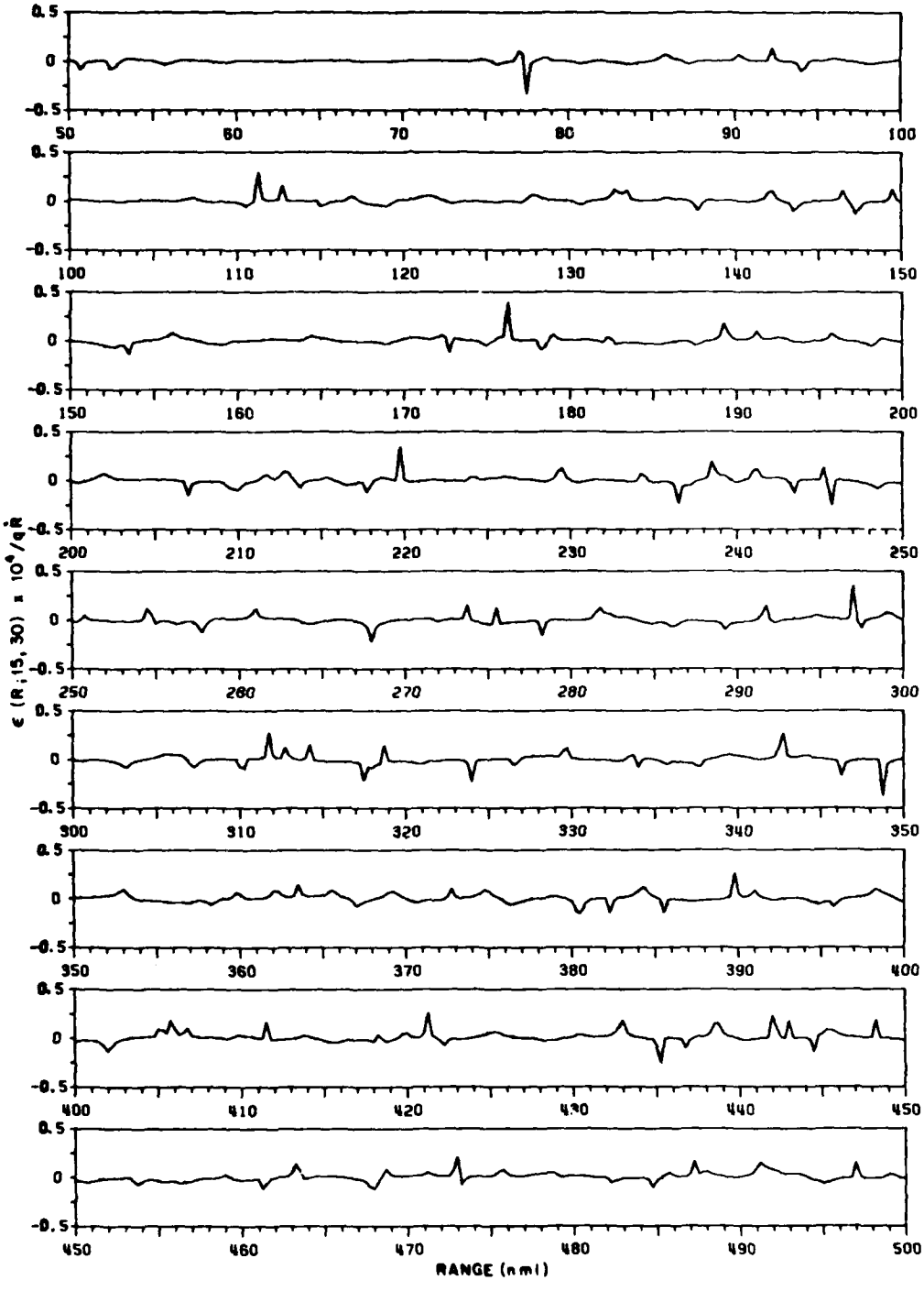

Fig. 30 — Dispersion measure $\epsilon \times 10^4/\dot{qR}$, over the range 50 to 500 nmi, between sinusoidal signals of 15 and 30 Hz. The measure of dispersion is the difference between the observed (or virtual) frequency ratio q' and the true frequency ratio q. $\dot{R}$ is the range rate in knots.

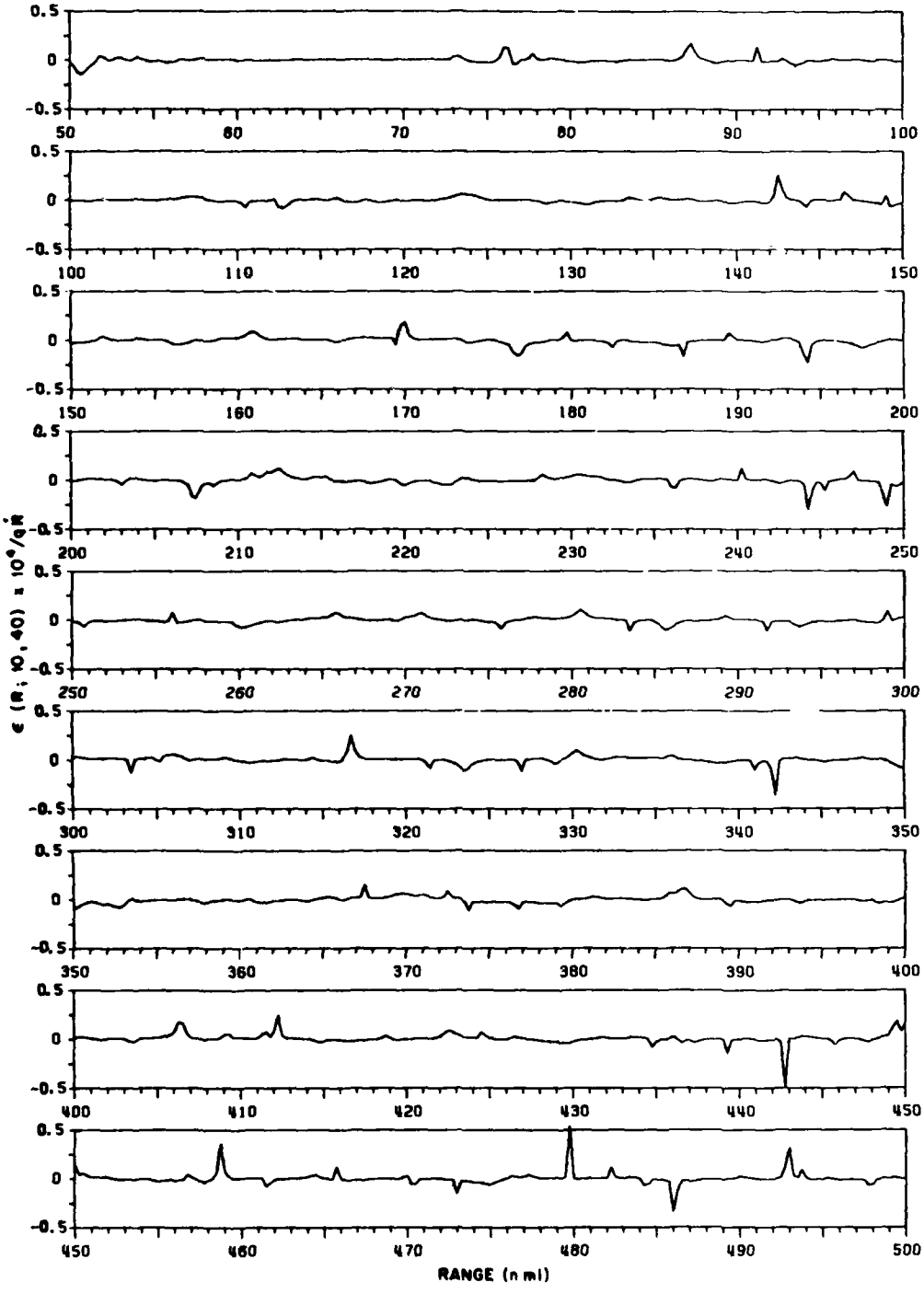

Fig. 31 — Dispersion measure $\epsilon \times 10^4 / qR$, over the range 50 to 500 nmi, between sinusoidal signals of 10 and 40 Hz. The measure of dispersion is the difference between the observed (or virtual) frequency ratio q' and the true frequency ratio q, $\dot{R}$ is the range rate in knots.

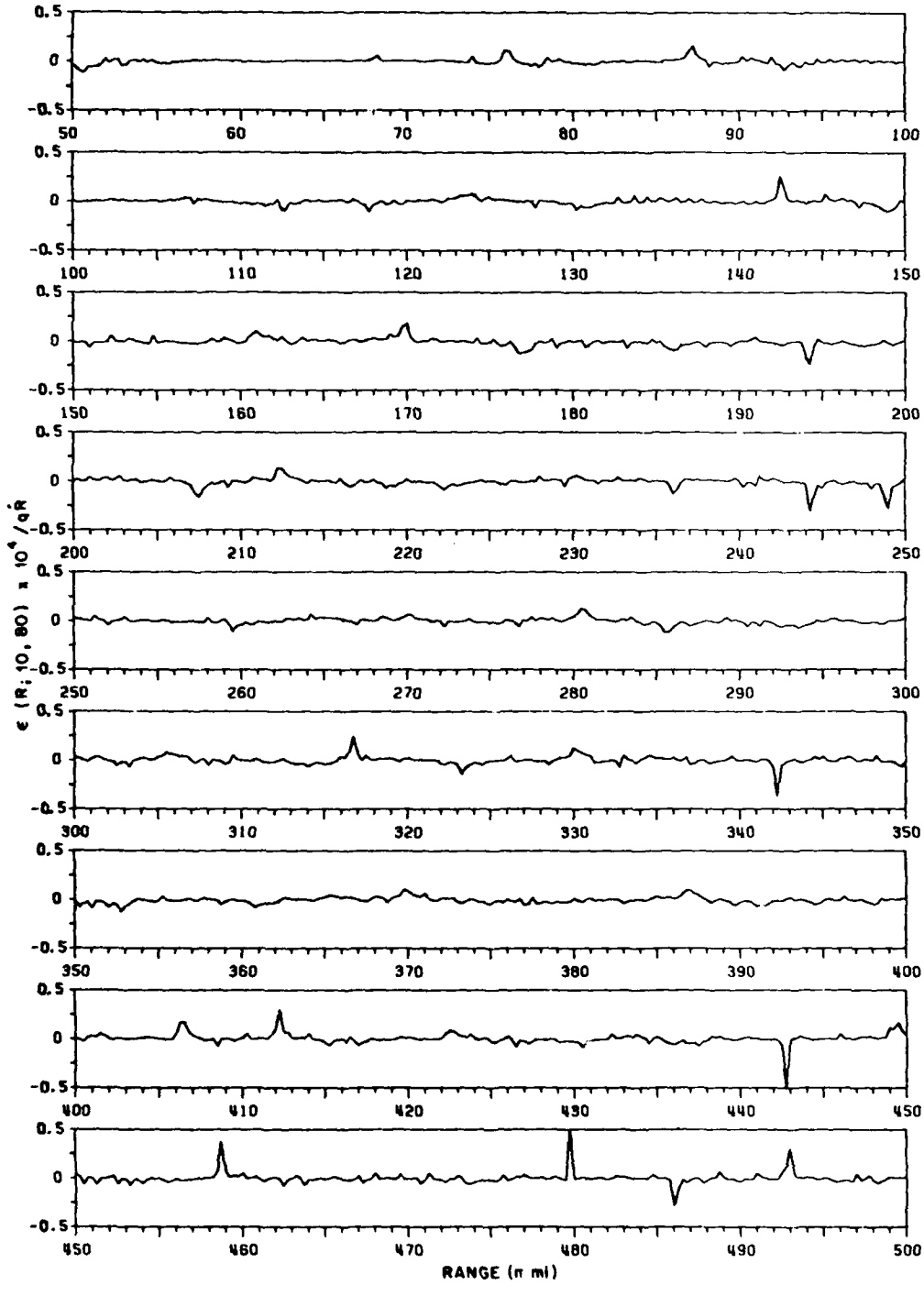

Fig. 32 — Dispersion measure $\epsilon \times 10^4 / q\dot{R}$, over the range 50 to 500 nmi, between sinusoidal signals of 10 and 80 Hz. The measure of dispersion is the difference between the observed (or virtual) frequency ratio q' and the true frequency ratio q. $\dot{R}$ is the range rate in knots.

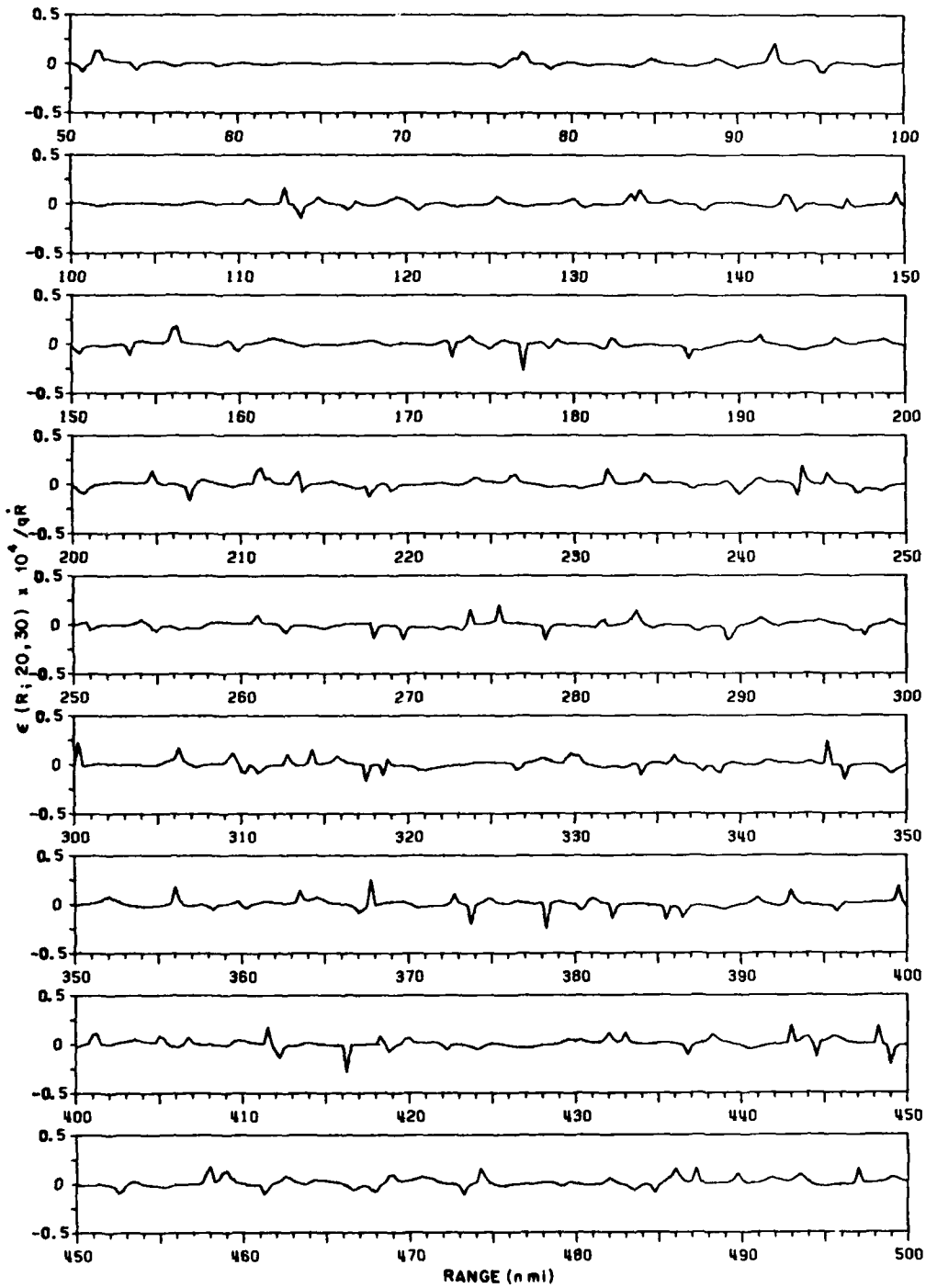

Fig. 33 — Dispersion measure $\epsilon \times 10^4 / q\dot{R}$, over the range 50 to 500 nmi, between sinusoidal signals of 20 and 30 Hz. The measure of dispersion is the difference between the observed (or virtual) frequency ratio q' and the true frequency ratio q; $\dot{R}$ is the range rate in knots.

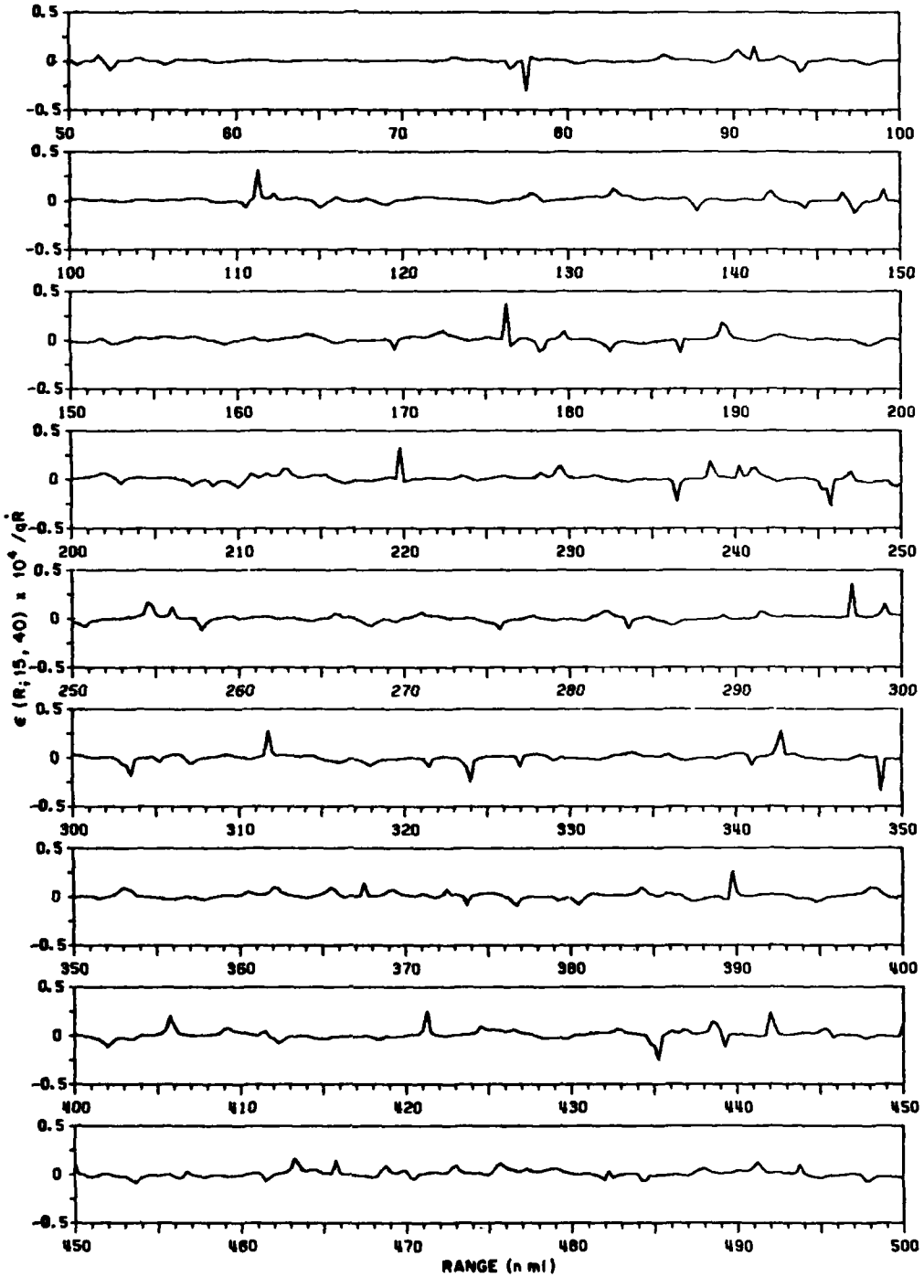

Fig. 34 — Dispersion measure $\epsilon \times 10^4 / q\dot{R}$, over the range 50 to 500 nmi, between sinusoidal signals of 15 and 40 Hz. The measure of dispersion is the difference between the observed (or virtual) frequency ratio q' and the true frequency ratio q. $\dot{R}$ is the range rate in knots.

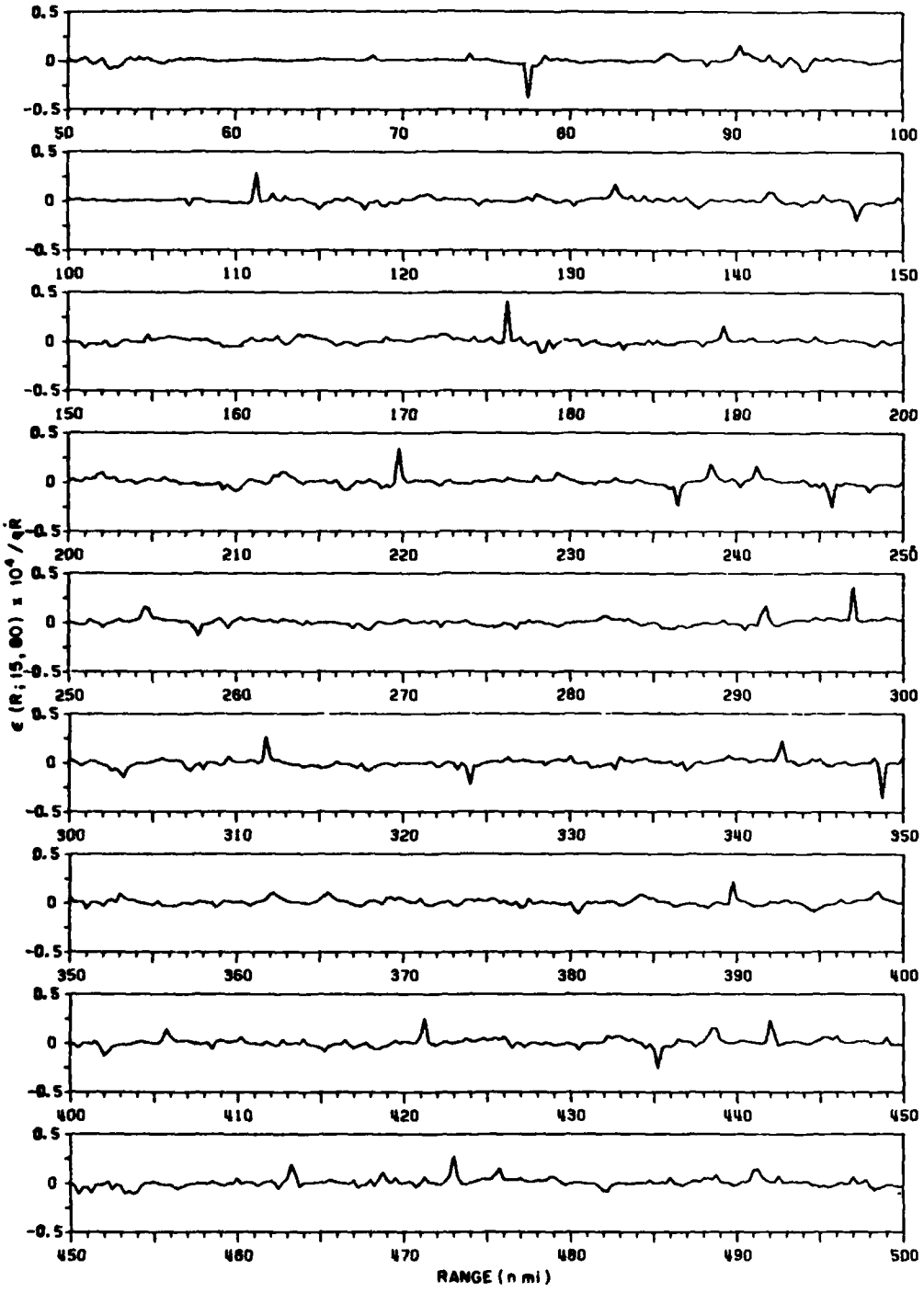

Fig. 35 — Dispersion measure $\epsilon \times 10^4 / q\dot{R}$, over the range 50 to 500 nmi, between sinusoidal signals of 15 and 80 Hz. The measure of dispersion is the difference between the observed (or virtual) frequency ratio q' and the true frequency ratio q; $\dot{R}$ is the range rate in knots.

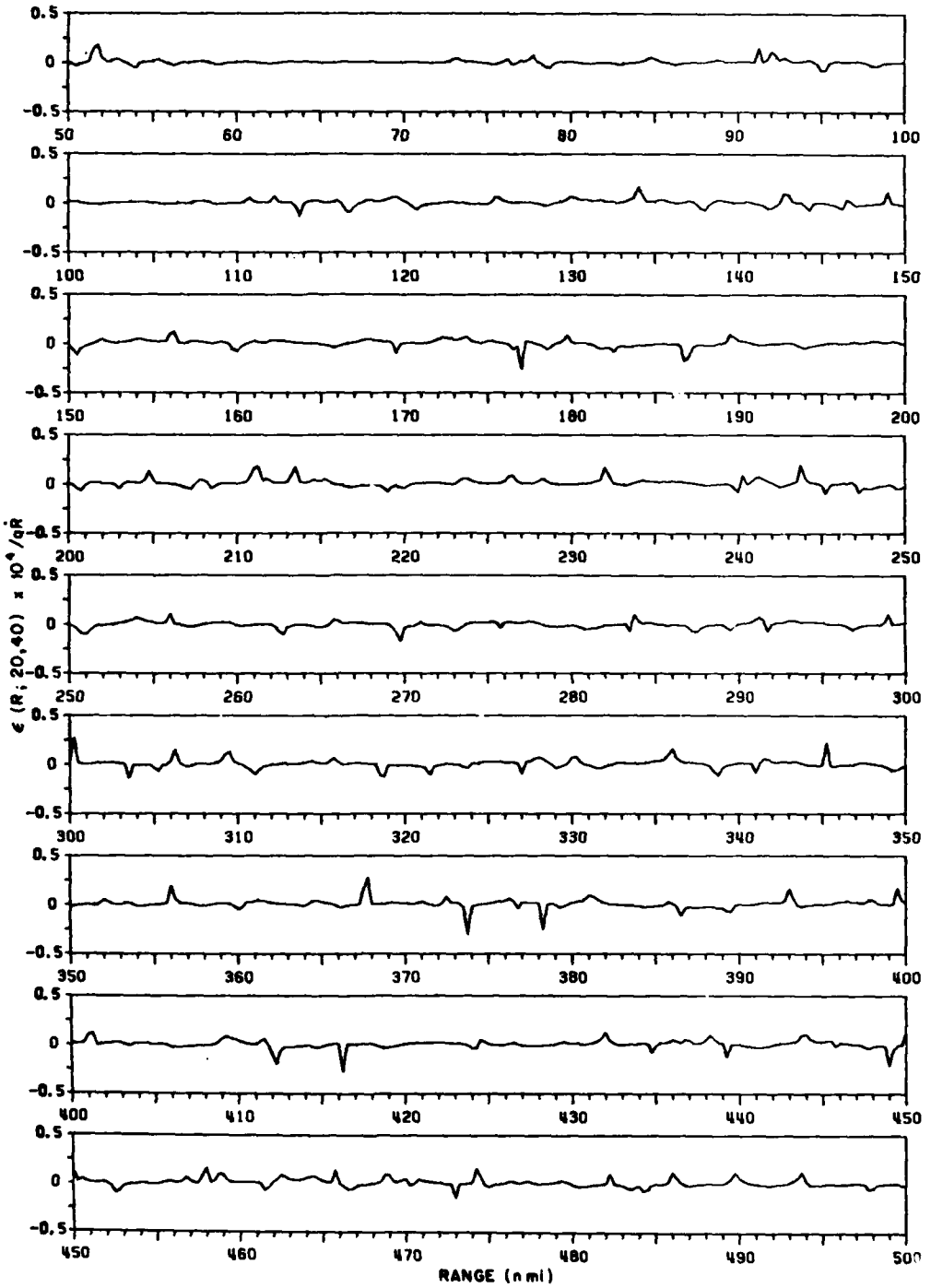

Fig. 36 — Dispersion measure $\epsilon \times 10^4/\dot{qR}$, over the range 50 to 500 nmi, between sinusoidal signals of 20 and 40 Hz. The measure of dispersion is the difference between the observed (or virtual) frequency ratio q' and the true frequency ratio q. $\dot{R}$ is the range rate in knots.

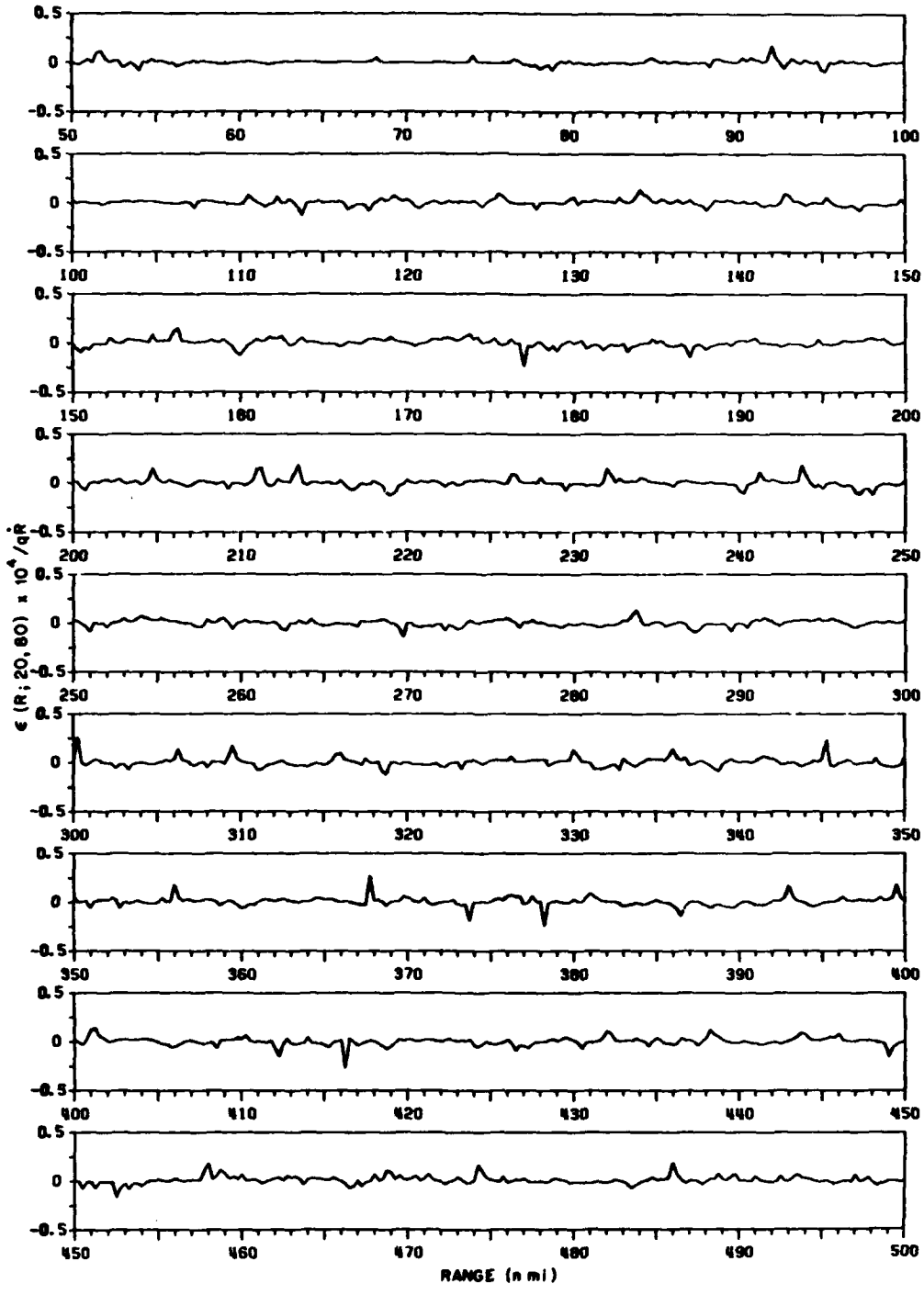

Fig. 37 — Dispersion measure $\epsilon \times 10^4/q\dot{R}$, over the range 50 to 500 nmi, between sinusoidal signals of 20 and 80 Hz. The measure of dispersion is the difference between the observed (or virtual) frequency ratio q' and the true frequency ratio q; $\dot{R}$ is the range rate in knots.

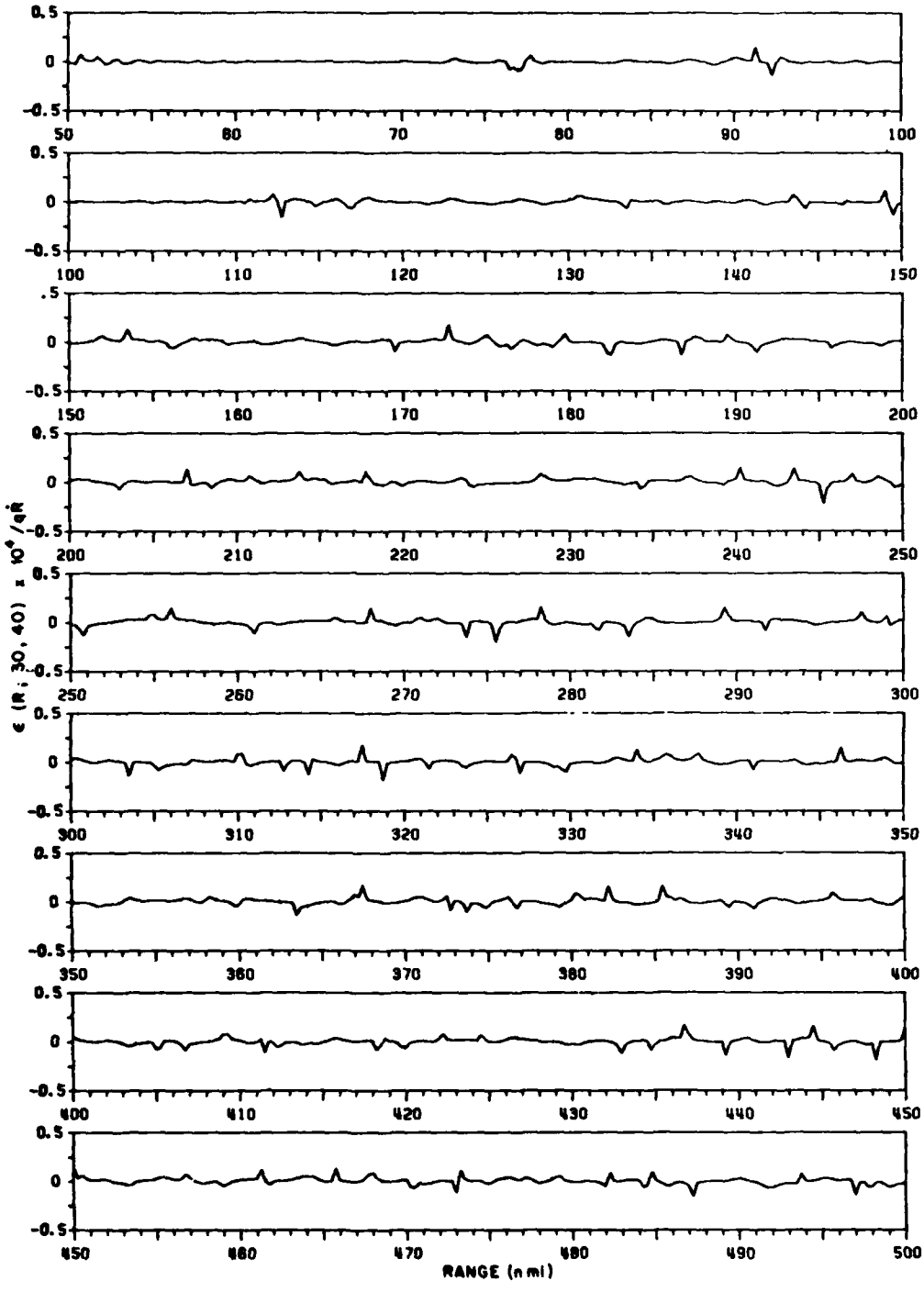

Fig. 38 — Dispersion measure $\epsilon \times 10^4 / q\dot{R}$, over the range 50 to 500 nmi, between sinusoidal signals of 30 and 40 Hz. The measure of dispersion is the difference between the observed (or virtual) frequency ratio q' and the true frequency ratio q. $\dot{R}$ is the range rate in knots.

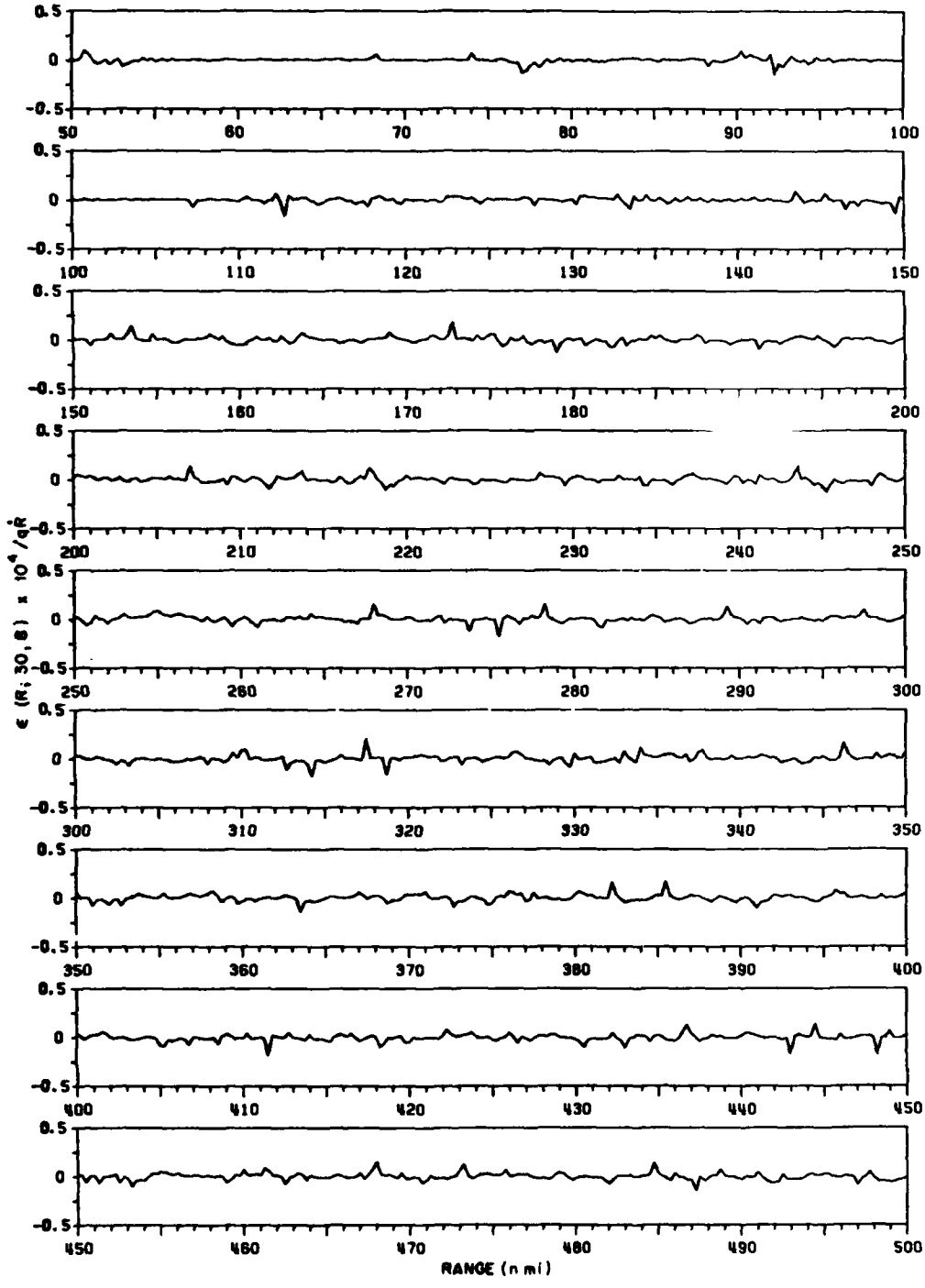

Fig. 39 — Dispersion measure $\epsilon \times 10^4 / q\dot{R}$, over the range 50 to 500 nmi, between sinusoidal signals of 30 and 80 Hz. The measure of dispersion is the difference between the observed (or virtual) frequency ratio q' and the true frequency ratio q. $\dot{R}$ is the range rate in knots.

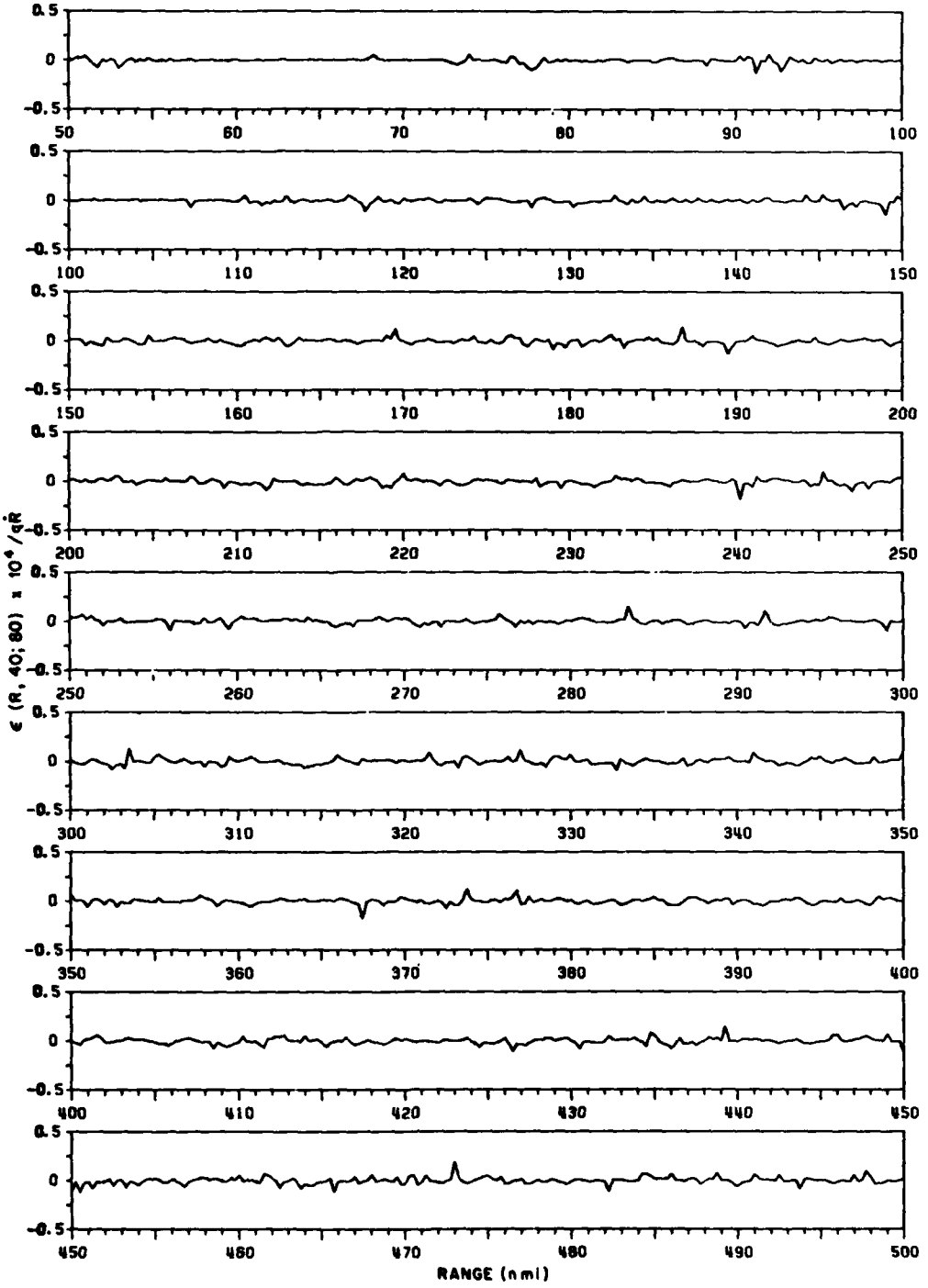

Fig. 40 — Dispersion measure $\epsilon \times 10^4 / q\dot{R}$, over the range 50 to 500 nmi, between sinusoidal signals of 40 and 80 Hz. The measure of dispersion is the difference between the observed (or virtual) frequency ratio q' and the true frequency ratio q, $\dot{R}$ is the range rate in knots.

DISTRIBUTION OF SPECTRAL DISPERSION MEASURE

An important measure to be obtained from the data on frequency dispersion is the distribution of $\epsilon(R; f_1, f_2)$ for the significant parameters under consideration. Histograms depicting the probability density of $\epsilon \times 10^6/q\dot{R}$ have been computed, over the range of 50 to 500 nmi, for each of the frequency pairs under consideration. They are displayed in Fig. 41. The histograms (from left to right and top to bottom) are ordered to display increasing values of the frequency ratio q. Since there appears to be no correlation between the histograms and the ratio q, it may be concluded that the spread of the distribution of ϵ is directly proportional to the frequency ratio q.

To study the correlation of the histograms with both range and signal frequency, the standard deviation of $\epsilon \times 10^6/q\dot{R}$ was computed, in 50-nmi range increments, for each signal frequency pair. The results are listed in Table 2. There appears to be a slight correlation of dispersion with range (as might be expected intuitively), and a somewhat stronger correlation with the frequencies of the signal pairs. In this latter case, however, the spread of the distribution is largely influenced by the peaks of the spikes of $\epsilon/q\dot{R}$ (see Figs. 26 through 40). If this influence is removed (by ignoring the spikes), the correlation of the distribution with signal frequency would be rather negligible.

Table 2 — Standard Deviation of $\epsilon \times 10^6/q\dot{R}$ Computed over 50-nmi Range Increments for 15 Signal-Frequency Pairs

	Standard Deviation									
Freq. Pair (Hz)	50 nmi to 100 nmi	100 nmi to 150 nmi	150 nmi to 200 nmi	200 nmi to 250 nmi	250 nmi to 300 nmi	300 nmi to 350 nmi	350 nmi to 400 nmi	400 nmi to 450 nmi	450 nmi to 500 nmi	50 nmi to 500 nmi
10-15	3.92	4.26	5.14	5.58	4.57	6.01	4.21	6.55	6.85	5.35
10-20	3.52	3.90	4.26	5.30	4.27	5.18	5.04	6.80	6.77	5.13
15-20	3.88	4.26	4.59	5.58	4.72	5.72	5.36	5.36	4.41	4.92
10-30	3.13	3.48	4.34	4.84	3.87	5.06	3.41	6.10	6.69	4.72
15-30	3.26	3.89	4.20	5.22	4.81	5.70	4.64	5.38	4.31	4.66
10-40	3.03	3.01	4.07	4.74	3.13	4.36	3.21	5.20	6.37	4.28
10-80	2.91	3.42	3.99	4.68	3.09	4.44	3.20	5.55	5.96	4.28
20-30	3.01	3.20	4.06	4.51	4.15	4.74	4.87	4.80	4.36	4.25
15-40	3.28	3.62	4.29	4.98	4.31	5.04	3.66	4.83	3.65	4.24
15-80	3.80	3.81	4.28	5.09	4.29	5.00	3.53	4.60	4.48	4.35
20-40	2.77	3.06	3.91	4.03	3.33	4.54	4.76	4.24	3.91	3.90
20-80	2.68	3.06	4.00	4.43	3.30	4.51	4.57	4.12	3.99	3.91
30-40	2.20	2.48	3.27	3.35	3.90	3.76	3.48	3.95	3.56	3.38
30-80	2.53	2.71	3.27	3.29	3.49	3.92	3.42	3.71	3.53	3.35
40-80	2.28	2.30	2.80	2.98	2.73	3.13	2.73	3.05	3.39	2.84
ALL	3.12	3.41	4.07	4.64	3.91	4.80	4.08	5.05	4.98	4.29

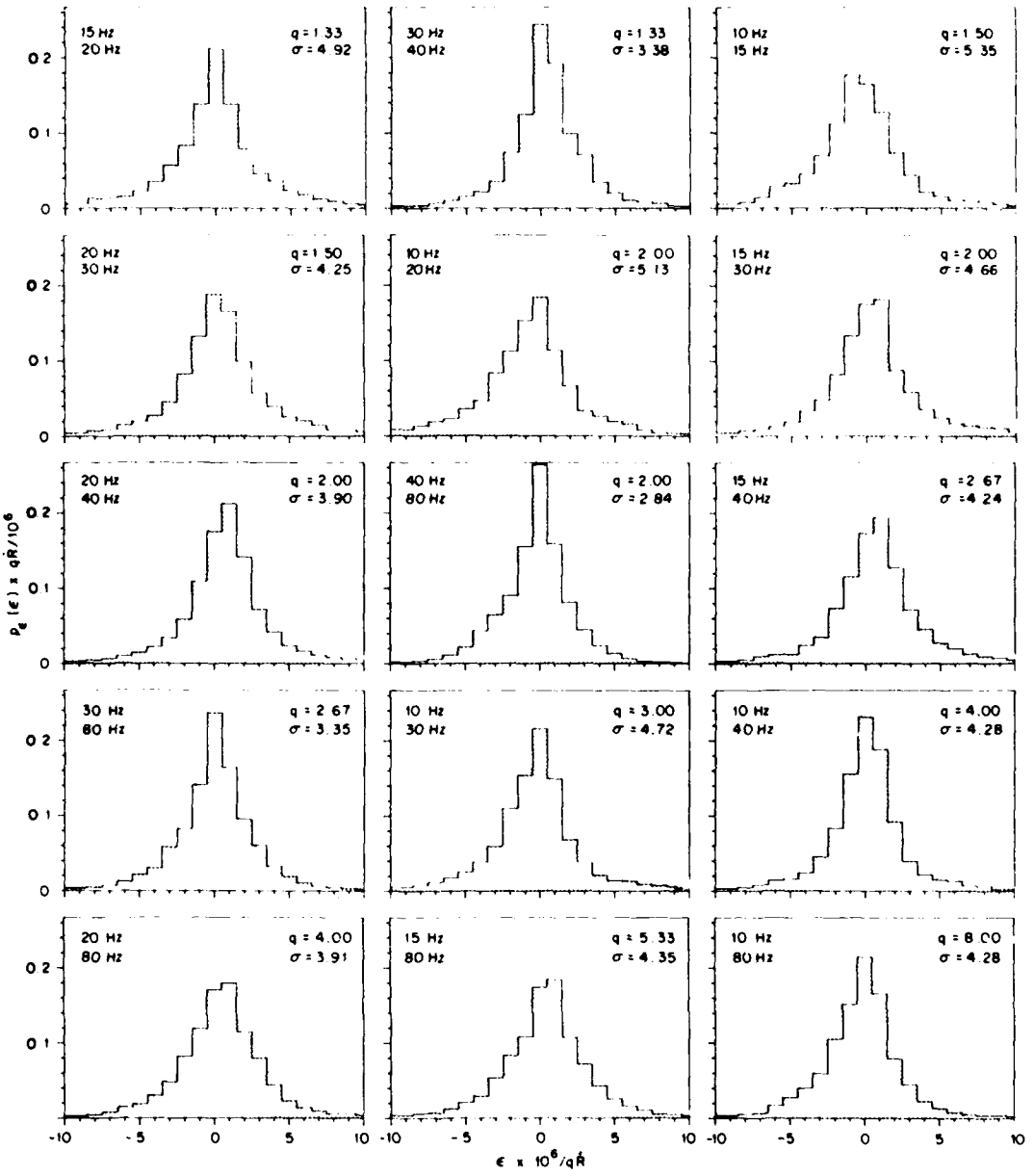

Fig. 41 — Histograms depicting the probability density of the spectral dispersion measure $\epsilon \times 10^6/\dot{qR}$ over the range 50 to 500 nmi for 15 pairs of signal frequencies. The histograms are ordered to display increasing values of the true frequency ratio q.

A histogram comprising all of the data is illustrated in Fig. 42, and the resulting cumulative probability diagram is illustrated in Fig. 43. The latter figure displays the probability that $\epsilon \times 10^6/q\dot{R}$ falls within plus or minus the given abscissa value. Thus, it is 90% probable that the virtual (or observed) frequency ratio q' will not deviate more than 5 $q\dot{R} \times 10^{-6}$ from the true frequency ratio q.

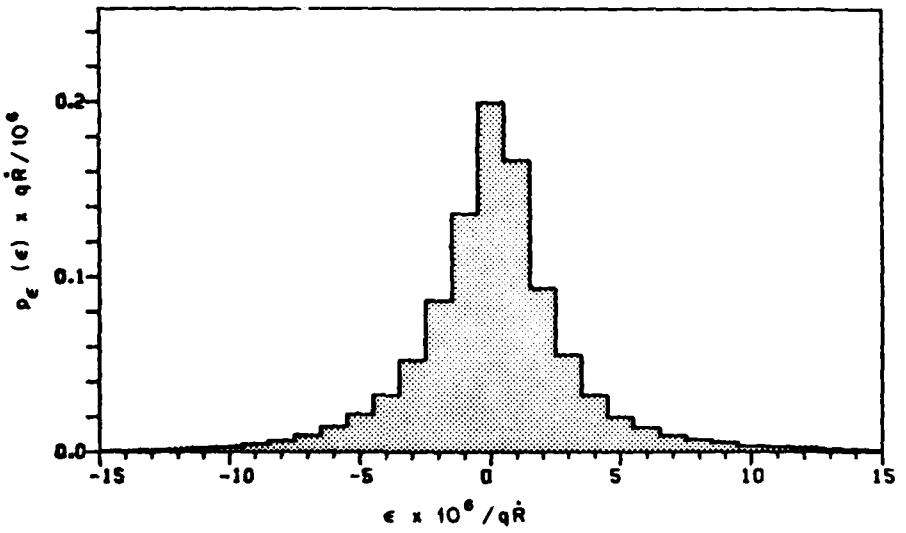

Fig. 42 — Histogram depicting the probability density of the spectral dispersion measure ϵ over the range 50 to 500 nmi. The histogram is the average of the histograms displayed in Fig. 41 and is assumed independent of the signal frequencies used.

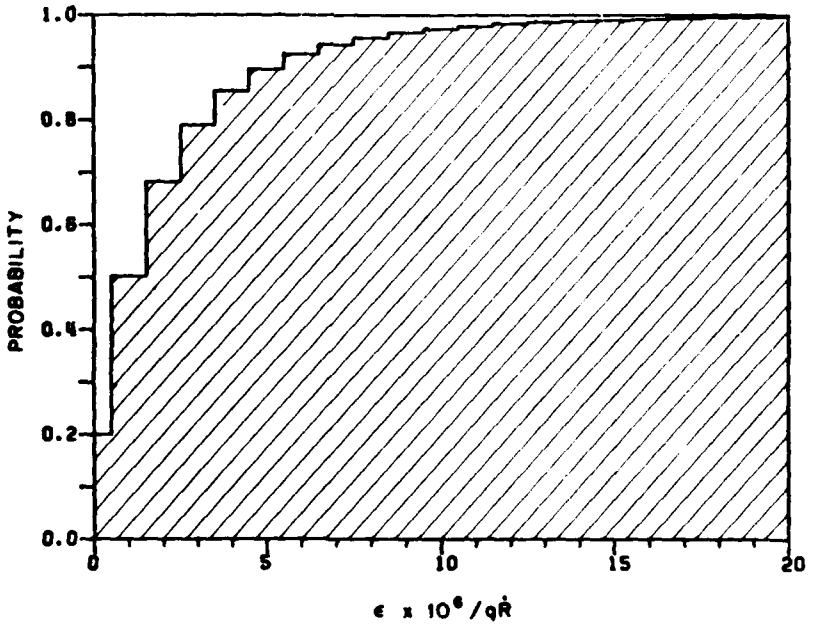

Fig. 43 — Cumulative probability of the dispersion measure ϵ about zero computed from the histogram displayed in Fig. 42

Another way of looking at the results is that ϵ/q is a measure of the time rate-of-change in the difference in virtual propagation time between two signals of different frequency [Eq. (10)]. As a consequence, when the abscissa of Fig. 43 is multiplied by $\dot{R}$ (in knots), one obtains the probability that the time rate-of-change in propagation time between the two signals will be equal to or less than the abscissa value in microseconds per second. Thus, it is 90% probable that the measure $|\epsilon/q|$ is not greater than $5\dot{R}\ \mu$s/s.

CONCLUSIONS

Acoustic dispersion in an ocean channel is manifested as a variation in the virtual phase-propagation speed with frequency along the radius of propagation. As a consequence, the virtual propagation time for sinusoidal signals varies both with range and with the frequency of the transmitted signal. When two such signals are transmitted, the observed (or virtual) frequency ratio, moving along the radius of propagation, will fluctuate about the true frequency ratio of the transmitted signals. The magnitude of these fluctuations is directly proportional to the transmitted frequency ratio. A measure of the spectral dispersion ϵ is defined as the difference between the virtual and the true frequency ratio q. The ratio ϵ/q, for a 1-knot range rate (reflecting the time rate-of-change of the difference in propagation time between two sinusoidal signals), is typically less than 5 μs/s. The dependence of this ratio on range (over the range of 50 to 500 nmi) and on the frequency of the signals (between 10 and 80 Hz) is found to be relatively insignificant (see Table 2 and Fig. 41). It can be concluded that spectral acoustic dispersion in a deep ocean channel is microscopic, but it can be significant for applications involving the phase correlation of broadband (or spectrally separated) signals over long time intervals.

ACKNOWLEDGMENT

This effort was supported by the Research and Technology Group (Code 612) of the Naval Electronic Systems Command under the management of John G. Schuster and Ronald Mitnick. The work was conducted under Work Request N0003982WRDW023.

REFERENCES

1. K.D. Flowers, "Geometric Dispersion of Acoustic Signals Propagated in a Deep Ocean Channel," *J. Acoust. Soc. Am.*, in press.

2. K.D. Flowers, "A Look at Remote Sensing of the Ocean Temperature Structure," NRL Memorandum Report 4461, March 1981.

3. R.P. Porter, "Transmission and Reception of Transient Signals in a SOFAR Channel," *J. Acoust. Soc. Am.* **54**(4), 1081-1091 (Oct. 1973).

4. R.P. Porter, "Dispersion of Axial SOFAR Propagation in the Western Mediterranean," *J. Acoust. Soc. Am.* **53**(1), 181-191 (Jan. 1973).

5. H.P. Bucker, "Normal-Mode Sound Propagation in Shallow Water," *J. Acoust. Soc. Am.* **36**(2), 251-258 (Feb. 1964).

6. H. Kutschale, "Long-Range Sound Transmission in the Arctic Ocean," *J. Geophys. Res.* **66**(7), 2189-2198.

7. I. Tostby, "Dispersion and Simple Harmonic Point Sources in Wave Ducts," *J. Acoust. Soc. Am.* **27**(5), 897-907 (Sept. 1955).

8. J.F. Miller and S.N. Wolf, "Modal Acoustic Transmission Loss (MOATL): A Transmission-Loss Computer Program Using a Normal Mode Model of the Acoustic Field in the Ocean," NRL Report 8429, Aug. 1980.

9. A.A. Gerlach, "Impact of the Ocean Acoustic Transfer Function on the Coherence of Undersea Propagations," *IEEE Trans. Acoust., Speech, Signal Process.* **ASSP-28**(2), 145-158 (Apr. 1980).

10. A.A. Gerlach, "Acoustic Transfer Function of the Ocean for a Motional Source," *IEEE Trans. Acoust., Speech, Signal Process.* **ASSP-26**(6), 493-501 (Dec. 1978).


DATE
FILME
8